

EDGE: Predictable Scatter in the Stellar Mass–Halo Mass Relation of Dwarf Galaxies

Stacy Y. Kim^{1,2*}, Justin I. Read², Martin P. Rey³, Matthew D. A. Orkney^{4,5}, Sushanta Nigudkar, Andrew Pontzen⁶, Ethan Taylor², Oscar Agertz⁷, Payel Das²

¹*Carnegie Theoretical Astrophysics Center, Carnegie Observatories, 813 Santa Barbara St, Pasadena, CA 91106, USA*

²*Department of Physics, University of Surrey, Guildford, GU2 7XH, UK*

³*Sub-department of Astrophysics, University of Oxford, DWB, Keble Road, Oxford OX1 3RH, UK*

⁴*Institut de Ciències del Cosmos (ICCUB), Universitat de Barcelona, Martí i Franquès 1, E-08028 Barcelona, Spain*

⁵*Institut d'Estudis Espacials de Catalunya (IEEC), E-08034 Barcelona, Spain*

⁶*Department of Physics and Astronomy, University College London, London WC1E 6BT, UK*

⁷*Lund Observatory, Division of Astrophysics, Department of Physics, Lund University, Box 43, SE-221 00 Lund, Sweden*

Accepted XXX. Received YYY; in original form ZZZ

ABSTRACT

The stellar-mass–halo-mass (SMHM) relation is central to our understanding of galaxy formation and the nature of dark matter. However, its normalisation, slope, and scatter are highly uncertain at dwarf galaxy scales. In this paper, we present **DarkLight**, a new semi-empirical dwarf galaxy formation model designed to robustly predict the SMHM relation for the smallest galaxies. **DarkLight** harnesses a correlation between the mean star formation rate of dwarfs and their peak rotation speed—the $\langle \text{SFR} \rangle - v_{\text{max}}$ relation—that we derive from simulations and observations. Given the sparsity of data for isolated dwarfs with $v_{\text{max}} \lesssim 20$ km/s, we fit the $\langle \text{SFR} \rangle - v_{\text{max}}$ relation to observational data for dwarfs above this velocity scale and to the high-resolution EDGE cosmological simulations below. Reionisation quenching is implemented via distinct $\langle \text{SFR} \rangle - v_{\text{max}}$ relations before and after reionisation. We find that the SMHM scatter is small at reionisation, ~ 0.2 dex, but rises to ~ 0.5 dex (1σ) at a halo mass of $\sim 10^9 M_{\odot}$ as star formation is quenched by reionisation but dark matter halo masses continue to grow. While we do not find a significant break in the slope of the SMHM relation, one can be introduced if reionisation occurs early ($z_{\text{quench}} \gtrsim 5$). Finally, we find that dwarfs can be star forming today down to a halo mass of $\sim 2 \times 10^9 M_{\odot}$. We predict that the lowest mass star forming dwarf irregulars in the nearby universe are the tip of the iceberg of a much larger population of quiescent isolated dwarfs.

Key words: cosmology – dark matter – galaxies: dwarf – galaxies: haloes

1 INTRODUCTION

The connection between dwarf galaxies and their dark matter haloes is key to many fundamental questions in astrophysics. This includes the lowest mass halo that can host a galaxy (Jethwa et al. 2018), how feedback regulates star formation in dwarf galaxies (e.g. Agertz et al. 2020), how many dwarfs should be observable in upcoming surveys (Danieli et al. 2018), how much dwarfs contribute to reionizing the universe (Weisz & Boylan-Kolchin 2017), and to what degree accreted dwarfs can shape the stellar haloes of Milky Way analogs (Rey & Starkenburg 2022). The galaxy-halo connection is also key for testing dark matter models with galaxy counts. Indeed, the long-standing ‘missing satellites problem’—a mismatch between the number of visible dwarf galaxies and the number of dark matter haloes predicted in the standard cold dark matter paradigm (Λ CDM; Klypin et al. 1999; Moore et al. 1999)—can be solved with one’s choice of the SMHM relation (e.g. Read et al. 2017; Jethwa et al. 2018; Kim et al. 2018; Read & Erkal 2019; Nadler et al. 2020).

However, the relation between galaxies and their dark matter haloes

is not well understood at the mass scale of dwarf galaxies, particularly below halo masses $\lesssim 10^{10} M_{\odot}$ (e.g. Garrison-Kimmel et al. 2017; Read et al. 2017). Many attempts have been made to quantify the simplest form of this relation, in which the stellar mass of a galaxy is a monotonically related to its dark matter halo mass—the stellar mass-halo mass relation (SMHM). Attempts to match observed galaxies to dark matter haloes via the ‘abundance matching’ approach (e.g. Vale & Ostriker 2004) works well for more massive galaxies (e.g. Behroozi et al. 2013). However, at dwarf scales, such models require the addition of significant stochasticity, which is not well understood (e.g. Garrison-Kimmel et al. 2017; Kim et al. 2018; Nadler et al. 2020). An alternative approach is to simulate the SMHM from first principles. However, this comes with its own challenges. The smallest stellar systems can have stellar masses approaching just $\sim 1000 M_{\odot}$ and sizes ~ 10 pc (Simon 2019), yet must be simulated over cosmologically representative volumes ($\gtrsim 50 \text{ Mpc}^3$) to obtain well-sampled galaxy population statistics. To date, no simulation has been able to capture this dynamic range, leaving a choice between large volume, lower resolution simulations such as Illustris and EAGLE (Genel et al. 2014; Schaye et al. 2015), or more targeted high resolution simulations that ‘zoom in’ on individual galaxies but lack

* E-mail: skim11@carnegiescience.edu (SYK)

full galaxy population statistics, such as EDGE (e.g. Chan et al. 2015; Wang et al. 2015; Jeon et al. 2017; Munshi et al. 2017; Agertz et al. 2020; Applebaum et al. 2021; Gutcke et al. 2022). It is perhaps not surprising, then, that current simulation results differ by two orders of magnitude below a halo mass of $10^{10} M_{\odot}$ (see Figure 8). There is also no consensus on the amount of scatter in such relations, with some predicting scatter of an order of magnitude, while others predict far less. Furthermore, most struggle to explain at least some of the observations. Recent high resolution simulations are now able to capture star-forming galaxies at a mass scale of $\sim 5 \times 10^9 M_{\odot}$ (Jeon et al. 2017; Rey et al. 2020; Applebaum et al. 2021; Gutcke et al. 2022), but none so far have a stellar mass as high as some isolated nearby dwarf irregulars such as Aquarius ($M_* \simeq 6.8 \times 10^5 M_{\odot}$) and CVnIdwA ($M_* \simeq 4.1 \times 10^6 M_{\odot}$; Read et al. 2017). It is not clear if this owes to a need to move to yet higher resolution, missing physics, a lack of population statistics, or difficulties in modelling and interpreting the data.

Despite these challenges, recent work has uncovered at least some of the likely sources of scatter in the SMHM relation at low mass. Using a novel “genetic modification” technique (Roth et al. 2016), Rey et al. (2019) showed, for the faintest dwarfs, the stellar mass is determined by how quickly the halo grows before reionisation, and can produce changes in its final stellar mass by as much as an order of magnitude. The interplay between reionisation and the scatter in dark matter assembly histories is thus a potentially significant contributor to the scatter in the SMHM at its faintest end. At the same time, Read & Erkal (2019) argued that additional scatter will be present for satellite dwarf galaxies if they quench (i.e. cease forming stars) on infall and/or experience significant mass loss through tides (see also Ural et al. 2015; Tomozeiu et al. 2016 for similar arguments). They argue that tidally-induced scatter is only significant if stellar mass loss is significant, which is rare¹, while the scatter due to quenching can also be removed if abundance matching is performed with a galaxy’s mean star formation rate, $\langle \text{SFR} \rangle$, averaged over the time the dwarf formed stars, rather than its stellar mass, M_* . Using data for nearby satellite dwarfs, they show that $\langle \text{SFR} \rangle$ correlates better with halo mass, M_{200} , than does M_* .

In this paper, we build on the above findings to present a new, fast, empirical galaxy-halo model, DarkLight. We improve on the $\langle \text{SFR} \rangle$ - M_{200} correlation presented in Read & Erkal (2019), showing that for very low mass dwarfs, $\langle \text{SFR} \rangle$ correlates more strongly with the peak rotation speed of a dwarf, v_{max} , than M_{200} . We then harness this new $\langle \text{SFR} \rangle$ - v_{max} relation to turn individual dark matter halo assembly histories, $v_{\text{max}}(t)$, into star formation histories (SFHs). Integrating the SFHs then returns the stellar mass of the dwarf, $M_*(t)$. We show that, once calibrated, this simple mapping is able to reproduce the stellar mass growth history of each of our simulated EDGE dwarfs over time. As we apply the mapping to all progenitors of the dwarf and track any accreted material, we are also able to reproduce any sudden jumps in stellar mass due to dry mergers.

DarkLight can be fully calibrated on measurements of $\langle \text{SFR} \rangle$ and v_{max} from nearby dwarf galaxies. This means that, with sufficiently good calibration data in hand, DarkLight need not rely on uncertain galaxy formation simulations, opening the door to robust cosmological constraints from dwarf galaxy number counts. At present,

however, a statistically significant sample of data is only available for dwarf galaxies with $v_{\text{max}} \gtrsim 20$ km/s. As such, here we calibrate DarkLight on observations above this velocity scale, and on the EDGE simulations below.

This paper is organised as follows. In Section 2, we present the details of DarkLight. In Section 3, we validate DarkLight by showing that it accurately reproduces the stellar mass evolution of individual EDGE dwarfs. Once calibrated, DarkLight only requires the growth history of a dark matter halo, and thus can be run on computationally inexpensive dark-matter-only (DMO) simulations of large cosmological volumes to predict the properties of large, statistical samples of dwarfs, down to the very smallest stellar systems. To illustrate this, in Section 4, we run DarkLight on a large, cosmological void volume (50 Mpc^3), to derive the SMHM relation *as if* we had run the entire volume with the resolution and baryonic physics model of EDGE. We study the origins of SMHM scatter and discuss the role of reionization in shaping the SMHM and its scatter and its sensitivity to changes in DarkLight’s input parameters. In Section 6, we study whether fully sampling over assembly histories in a large cosmological volume is sufficient to explain puzzling low mass star-forming galaxies in the nearby Universe such as Aquarius and CVnIdwA. We discuss our results, compare DarkLight against other galaxy formation models and hydrodynamic simulations, and outline its limitations in Section 7. Finally, in Section 8, we present our conclusions.

2 DARKLIGHT

Dwarf galaxies represent the extreme end of galaxy and star formation. As such, they remain a challenge to model numerically and are highly sensitive to the assumed subgrid physics (e.g. Munshi et al. 2019; Agertz et al. 2020). Galaxy formation models calibrated to reproduce massive galaxies often fail when run in the dwarf regime without modification (e.g. discussion in Sec. 7), indicating that different processes become important at low-mass scales. Here, we present a new model, DarkLight, that is tailored to accurately predict dwarf galaxy properties. DarkLight is based on two recent findings regarding the formation of dwarfs: (i) that, for reionisation-quenched dwarfs, dark matter assembly histories are particularly important in determining their stellar content (Rey et al. 2019); and (ii) that their star formation rates correlate with halo properties (Read & Erkal 2019). In Section 2.1, we discuss the latter and present a new $\langle \text{SFR} \rangle$ - v_{max} relation based on observed and simulated dwarf galaxies upon which DarkLight is based. In Section 2.2, we discuss how we apply this relation to the assembly histories of dwarf haloes to predict their stellar content over time. DarkLight is open-source and available to download at <https://github.com/stacykim/darklight>.

2.1 The $\langle \text{SFR} \rangle$ - v_{max} relation at dwarf scales

Read & Erkal (2019) showed that mean star formation rate, $\langle \text{SFR} \rangle$, of the Milky Way’s classical dwarf galaxies, and nearby dwarf irregulars, correlates tightly with halo mass, M_{200} . We find that there is considerably less scatter when relating $\langle \text{SFR} \rangle$ s to the maximum of the rotation curve, v_{max} (often used as a proxy for mass; e.g. Boylan-Kolchin et al. 2012) rather than halo mass, M_{200} (see Appendix A). This is due to two main effects. Firstly, v_{max} is better constrained in observations and less susceptible to mergers and environmental effects. Secondly, the star formation rate better correlates with the inner mass distribution (since this is where the gas and stars reside), which is better constrained by v_{max} than M_{200} . For these reasons,

¹ Evidence for tidal stripping has been reported for a few Milky Way dwarfs (e.g. Ibata et al. 2001; Pace et al. 2022; De Leo et al. 2023; Ou et al. 2024). Of these, only the Sagittarius dwarf shows evidence for significant stellar mass loss. However, even in this case we can correct for this stellar mass loss using Sagittarius’s detected tidal debris (Gibbons et al. 2017).

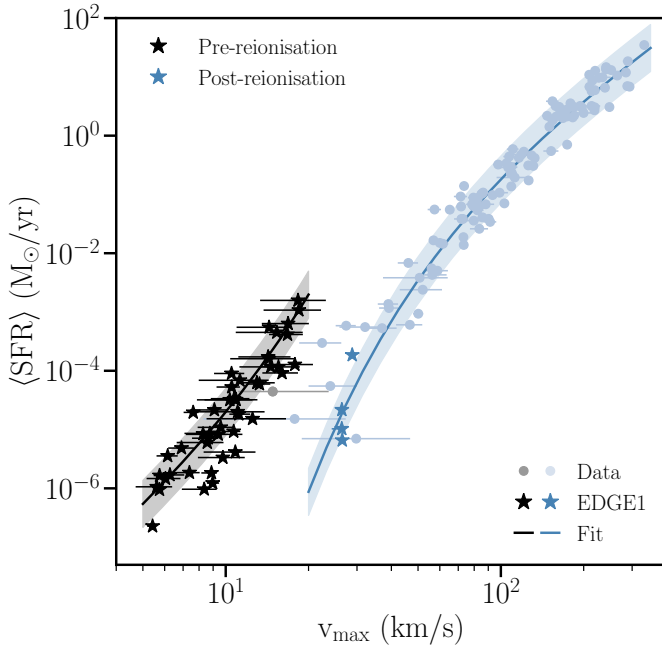


Figure 1. Relation between the average star formation rate and v_{max} . We find two relations: one pre-reionisation, shown in black, and another, with suppressed star formation rates, post-reionisation, shown in blue. The circles are derived from observational data (see Sec. 2.1 for details), while the stars are from the high-resolution cosmological EDGE suite of simulations. The dwarf galaxy represented by the gray circle just above $v_{\text{max}} \sim 10$ km/s is Eridanus II. In effect, the post-reionisation relation is calibrated by observational data, while the pre-reionisation relation is calibrated on the EDGE simulations.

in this paper we use the correlation between $\langle \text{SFR} \rangle$ and v_{max} , rather than the weaker correlation between $\langle \text{SFR} \rangle$ and M_{200} .

As reionisation suppresses or even halts star formation in dwarf galaxies, we construct a separate $\langle \text{SFR} \rangle$ - v_{max} relation before and after reionisation quenching. To construct the post-reionisation relation, we largely rely on data from observed nearby isolated galaxies. For galaxies with $v_{\text{max}} \gtrsim 20$ km/s, we use the observational sample of (non-rogue) dwarf irregulars in Read et al. (2017), which have stellar masses and v_{max} derived from photometric light profiles and HI rotation curves. A few of these galaxies have detailed star formation histories derived from deep color-magnitude diagrams. These include the dwarfs WLM (Albers et al. 2019), Aquarius (Cole et al. 2014), Leo T (Weisz et al. 2012), and IC 1613² (Skillman et al. 2014). For these four galaxies, we calculated their $\langle \text{SFR} \rangle$ s averaged over the last 1 Gyr. For the remainder of the dwarfs, that do not have detailed star formation histories, we calculated their mean lifetime star formation rates $\langle \text{SFR} \rangle = M_*/t_H$, where M_* is the stellar mass and t_H the Hubble time, based on stellar masses derived by Zhang et al. (2012) from SED fitting (c.f. the similar analysis adopted in Read et al. 2017 and Read et al. 2019).

We supplement these dwarfs with the SPARC dataset of disk galaxies. As detailed star formation histories are not available for these galaxies, we again compute their mean lifetime star formation rates

² Note that IC1613 is actually classed as a rogue in Read et al. (2017). However, we can use it here since, combining is stellar and HI gas kinematics, its inclination is determined robustly, allowing for a trustworthy inference of v_{max} (Oman et al. 2016; Collins & Read 2022).

based on stellar masses derived from their $3.6 \mu\text{m}$ luminosities published in Lelli et al. (2016) and stellar mass-to-light ratios published in Posti et al. (2019). For v_{max} , we use v_{flat} calculated by Lelli et al. (2016) based on HI/H α rotation curves.

Observational data on dwarfs with $v_{\text{max}} \lesssim 20$ km/s is sparse. While there are many observed dwarfs below this threshold, most are satellite galaxies, for which quenching and tidal stripping may have significantly affected their star formation histories. Restricting to isolated dwarf galaxies leaves us with one good candidate, Eridanus II (Li et al. 2017). Eridanus II has a very old stellar population that appears to have been quenched at about $t_{\text{quench}} = 2$ Gyr (Simon et al. 2021). We computed its $\langle \text{SFR} \rangle = M_*^{\text{EriII}} / t_{\text{quench}} = 4.44 \times 10^{-5} M_{\odot}/\text{yr}$. As its star formation history is consistent with being a reionisation relic, we used it in our fits for the pre-reionisation relation.

To supplement these data, we compiled $\langle \text{SFR} \rangle$ and v_{max} from the Engineering Dwarfs at Galaxy formation’s Edge (EDGE) simulation suite of low-mass dwarfs with halo masses $M_{200} = 1 - 4 \times 10^9 M_{\odot}$ (Agertz et al. 2020; Rey et al. 2019; Orkney et al. 2021). These fully cosmological zoom-in simulations are run with the adaptive mesh refinement code RAMSES (Teyssier 2002) and adopt the cosmological parameters $\Omega_M = 0.309$, $\Omega_{\Lambda} = 0.691$, $\Omega_b = 0.045$, and $H_0 = 67.77$ km/s/Mpc (Planck Collaboration et al. 2014). They have a maximum spatial resolution of 3 pc and self-consistently resolve the momentum and energy deposition from individual supernovae explosions. Dark matter is represented by particles with a mass resolution of $960 M_{\odot}$. Reionisation heating is modeled via an updated version of Haardt & Madau (1996) with a high-redshift cutoff implemented in the publicly available version of RAMSES. Reionisation begins at $z \sim 6.5$, but star formation fully quenches at $z_{\text{quench}} = 4$. A more complete description of the subgrid physics and the EDGE simulations is given in Agertz et al. (2020) and Rey et al. (2020). Halos are identified using the HOP halo finder (Eisenstein & Hut 1998), and merger trees constructed by matching halos between snapshots using pynbody (Pontzen et al. 2013) and tangos (Pontzen & Tremmel 2018). Halo masses M_{200} are defined as the mass within a radius r_{200} that encloses an average density that is 200 times the critical density of the universe.

For EDGE, we compute pre-reionisation values for all isolated galaxies that exist in our high-resolution volume at z_{quench} . We average the (in-situ) star formation rate and v_{max} from the birth times of each halo to z_{quench} . The v_{max} is computed at each time step from rotation curves based on all particles in the simulation. For those haloes that form stars again (i.e. “rejuvenate”, Wright et al. 2019; Rey et al. 2020) after reionisation, we compute the average star formation rate and v_{max} from the time they rejuvenate to the present day, and use these to fit the post-reionisation relation. There are more pre-reionisation than post-reionisation data points from EDGE due to the fact that there are many isolated galaxies before reionisation (many of which eventually merge with the main progenitor by $z = 0$), and because few of the EDGE dwarfs are rejuvenators.

Fits to the resultant dataset are shown in Fig. 1. Observational data are represented by circles, while simulation data are represented by stars. The pre-reionisation relation is shown in grey, while the post-reionisation relation is shown in blue. Where the EDGE and the observational data overlap, they agree well. The best-fit pre-reionisation relation is given by:

$$\langle \text{SFR} \rangle = 2 \times 10^{-7} \left(\frac{v_{\text{max}}}{5} \right)^{3.75} e^{v_{\text{max}}/5} M_{\odot} \text{ yr}^{-1} \quad (1)$$

with a 1σ symmetric scatter of 0.4 dex. Notice that the relation flattens slightly towards low v_{max} . The best-fit post-reionisation relation

is given by:

$$\langle \text{SFR} \rangle = 7.06 \left(\frac{v_{\text{max}}}{182.4} \right)^{3.07} e^{-182.4/v_{\text{max}}} \text{ M}_{\odot} \text{ yr}^{-1} \quad (2)$$

with a 1σ symmetric scatter of 0.3 dex. These two relations are shown in Fig. 1 as black and blue lines, respectively, with the 1σ scatter marked by bands.

2.2 Constructing dwarf galaxies

We can now apply the $\langle \text{SFR} \rangle$ - v_{max} relation from Section 2.1 to generate star formation histories, $\text{SFR}(t)$, and stellar masses, $M_*(t)$, from the $v_{\text{max}}(t)$ trajectory of a halo drawn from a dark matter only simulation. We correct the $v_{\text{max}}(t)$ trajectory to subtract the baryonic contribution (much of which is evaporated away for the lowest-mass dwarfs during reionisation) by multiplying by $\sqrt{1 - f_b}$, where $f_b = \Omega_b/\Omega_m = 0.17$ is the baryon fraction of the universe. In Appendix B, we show that this provides a better match to the v_{max} the halo would have had if it had been run in a hydrodynamic simulation. We take the average v_{max} before reionisation and use the pre-reionisation $\langle \text{SFR} \rangle$ - v_{max} relation (the relation in black/gray in Fig. 1) to derive a single, average pre-reionisation SFR before reionization quenching, $z < z_{\text{quench}}$. After $z > z_{\text{quench}}$, haloes do not form stars unless/whenever they pass above a threshold $v_{\text{max}}^{\text{post}}$, upon which we assign a single, average SFR based on the halo's v_{max} at $z=0$ from the post-reionisation relation (the relation in blue in Fig. 1). For each timestep in which star formation occurs after reionisation, we add scatter from the appropriate $\langle \text{SFR} \rangle$ - v_{max} relation.

The above procedure produces a stellar mass trajectory for stars formed in-situ, $M_*(t)$. In addition, we calculate the contribution from accreted haloes by running DarkLight on all haloes that merge onto the main halo. Optionally, one can impose a halo occupation function to capture the suppression of galaxy formation in low-mass halos, which have limited ability to accrete and cool star-forming gas, particularly after reionisation. In this case, whether each accreted halo contains a galaxy or not is probabilistically determined from the halo occupation function. By default, DarkLight does not adopt a halo occupation function.

For any given halo, DarkLight can generate multiple realisations of the halo's stellar mass growth history, sampling the scatter in the $\langle \text{SFR} \rangle$ - v_{max} relation and yielding confidence intervals on $M_*(t)$.

3 VALIDATION: REPRODUCING HYDRODYNAMIC SIMULATIONS

In this section, we show how DarkLight reproduces the stellar mass growth history, $M_*(t)$, of the fully hydrodynamic, high-resolution dwarf galaxies in the EDGE suite. To do this, we first extracted the $v_{\text{max}}(t)$ trajectories for each of the dwarfs from DMO zoom simulations. We then smoothed the trajectories with a 1 Gyr Gaussian filter to remove small fluctuations in $v_{\text{max}}(t)$ that occur due to mergers/interactions and calculated $\text{SFR}(t)$ based on the smoothed trajectories using DarkLight.

The results are shown in Fig. 2. We find that $v_{\text{max}} = 26.3$ km/s and $z_{\text{quench}} = 4$ reproduce the EDGE dwarfs well. The upper panels of each row show the original $v_{\text{max}}(t)$ trajectories from EDGE with a gray line. These are smoothed (blue line) before being input to DarkLight. The star formation histories from EDGE and DarkLight are overplotted as gray and blue histograms, respectively. The bottom panels show the evolution of the total stellar mass

in EDGE versus DarkLight in black and dark blue lines, respectively. The stellar mass formed in-situ in EDGE versus DarkLight is shown in gray and light blue lines, respectively. The bands denote the 1 and 2σ scatter in the range of predicted stellar masses based on 100 realizations of each halo. For most haloes, the median $M_*(t)$ produced by DarkLight matches the stellar mass trajectories in EDGE within 2σ . This includes an excellent recovery of reionisation-quenched dwarfs like Halo 1445 and Halo 1449, and ‘rejuvenators’ that reignite their star formation sometime after reionisation like Halo 600 and Halo 605 (see also Rey et al. 2020, for a discussion of rejuvenation).

However, late-forming haloes that are built up by many small mergers (typically $\sim 2\sigma$ outliers) are less well reproduced (e.g. Haloes 600lm and 1459mr02). This is due to the difficulty of reproducing the stellar masses of the very low mass haloes ($M_{200} \lesssim 10^8 \text{ M}_{\odot}$) they merge with, which is in turn caused by difficulties in measuring v_{max} for such haloes. However, even in these scenarios, the final stellar masses are reproduced to within a factor of a few. We discuss how we can improve upon this in future work in Sec 7.3.

4 THE STELLAR-MASS–HALO-MASS RELATION

In this section, we present a first application of DarkLight by applying it to the dark-matter-only (DMO) simulation of the void volume from which the EDGE dwarf galaxies were selected. This volume was selected from a DMO cosmological simulation with a box size of 50 Mpc and a resolution of 512^3 particles. We ran DarkLight on all haloes that did not have a merger history indicative of a close encounter with a more massive halo (i.e. that showed no unusual jumps or discontinuities in their mass growth history). In this way, we populate the entire void as if we had run EDGE on every galaxy in the volume.

In Fig. 3, we show DarkLight’s prediction for the SMHM relation of this void volume as grey points, plotting the median stellar mass obtained from integrating 100 realizations of the SFH for each halo. Overplotted are results from recent observational, simulation, and abundance matching studies. Observational data from isolated gas-rich dwarf irregulars, with halo masses inferred from their HI rotation curves from Read et al. (2017) are plotted with magenta stars. The black stars show galaxies from the EDGE simulations presented in Fig. 2—families of haloes created by genetically modifying a single halo to form earlier or later appear as vertical lines of points. Those from NIHAO (Wang et al. 2015), FIRE (Chan et al. 2015; Wheeler et al. 2015; Wetzel et al. 2016; Fitts et al. 2017), and the Marvelous and DC Justice League (Munshi et al. 2021) simulation suites are shown as green circles, blue squares, and red triangles, respectively. Abundance-matching relations from Behroozi et al. (2013) and Moster et al. (2013) are shown by the yellow and orange lines, respectively.

At halo masses $M_{200} \gtrsim 10^{10} \text{ M}_{\odot}$, the differences between all of the studies, including DarkLight, are small. However, at halo masses $M_{200} \lesssim 10^{10} \text{ M}_{\odot}$, the differences between the studies grow. Notably, the simulations predict that galaxies have significantly less stellar mass for a fixed halo mass than the observed galaxies (magenta), with differences as large as two orders of magnitude at the lowest masses. Furthermore, the differences between simulation suites are also large, with disagreement in not just the normalisation but also in the slope and scatter of the SMHM relation (as also observed by Garrison-Kimmel et al. 2017).

In contrast, DarkLight straddles the space between simulations and observations. We discuss possible reasons for the discrepancies

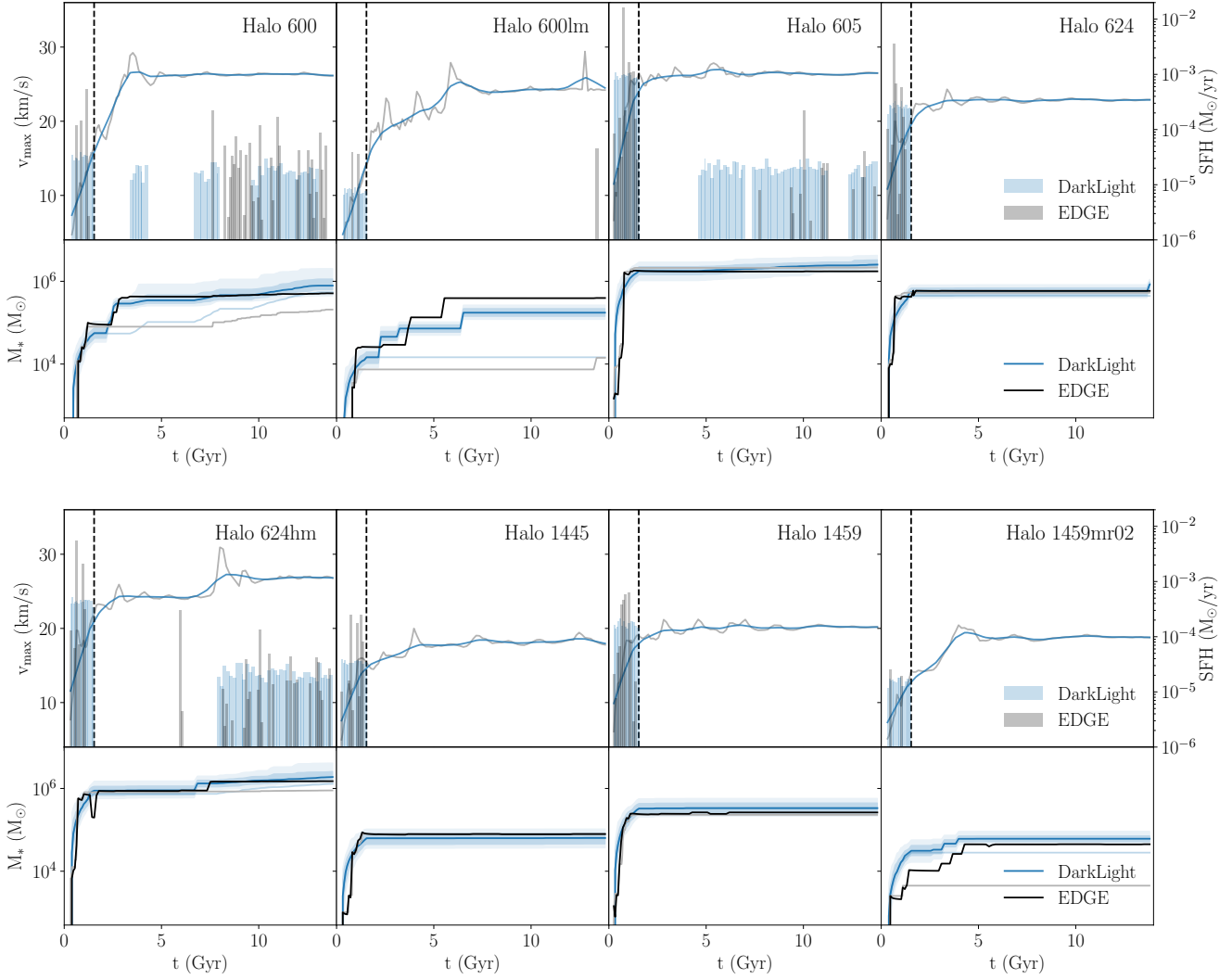


Figure 2. DarkLight’s prediction for the star formation histories and stellar mass trajectories, $M_*(t)$, for several EDGE dwarfs. In each row, the lines in the top panels denote the v_{\max} evolution of different haloes. The v_{\max} trajectories from the EDGE simulations is shown in gray. These trajectories are smoothed (blue lines) before being fed into DarkLight. Dashed black vertical lines denote $z_{\text{quench}} = 4$, when reionisation shuts off star formation in the lowest mass EDGE dwarfs. Star formation histories from EDGE and DarkLight are overplotted as gray and blue histograms, respectively. The bottom panels of each row show the cumulative stellar mass growth of several EDGE dwarf galaxies predicted by DarkLight (blue) compared to EDGE simulations of each (black). The black and dark blue lines denote the total stellar mass growth (in-situ and accreted), while the gray and light blue lines denote in-situ stellar mass growth (note that the in-situ mass trajectories do not include stellar mass loss, and thus can be higher than the total mass). The dark and light blue bands on the DarkLight stellar mass trajectories show the 1- and 2- σ range based on 100 DarkLight realisations of each halo’s SFR, accounting for the scatter in the SFR- v_{\max} relation. Note that the stellar masses predicted by DarkLight are accurate to within 2σ , and within a factor of two of the hydrodynamic simulations for all cases. The worst recovery is for late-forming haloes (Halo 600lm and Halo 1459mr02) that are built up by many small mergers ($M_{200} \leq 10^8 M_{\odot}$) for which the v_{\max} are difficult to measure.

between DarkLight and the different simulations in Section 7.2. DarkLight suggests that the lowest mass HI-rich dwarfs (magenta) are outliers in stellar mass for their halo mass—the tip of the iceberg of a large population of quenched dwarf galaxies with lower stellar masses that remain to be discovered. This implies that abundance matching relations based on this sample of observed dwarfs likely suffer from incompleteness and over- (under-) estimate stellar (halo) masses, as was found for Behroozi et al. (2013)’s relation for higher-mass dwarf galaxies (Garrison-Kimmel et al. 2014).

Some studies have found that the SMHM relation appears to have

a “knee” below which the relation steepens in slope. The location of the knee varies from study to study, ranging from $M_{200} = 10^{10} M_{\odot}$ (Munshi et al. 2021, for their “all haloes” SMHM relation) to $10^{11} M_{\odot}$ (Nadler et al. 2020; Danieli et al. 2023). We find that DarkLight does not predict a clear knee given our fiducial model parameters. However, we show in Section 4.2 that we can generate a stronger knee by shifting the redshift at which dwarf galaxies quench earlier. One can also be generated by decreasing pre-reionisation and/or increasing post-reionisation star formation rates to create a break at this mass scale. This occurs around where the popula-

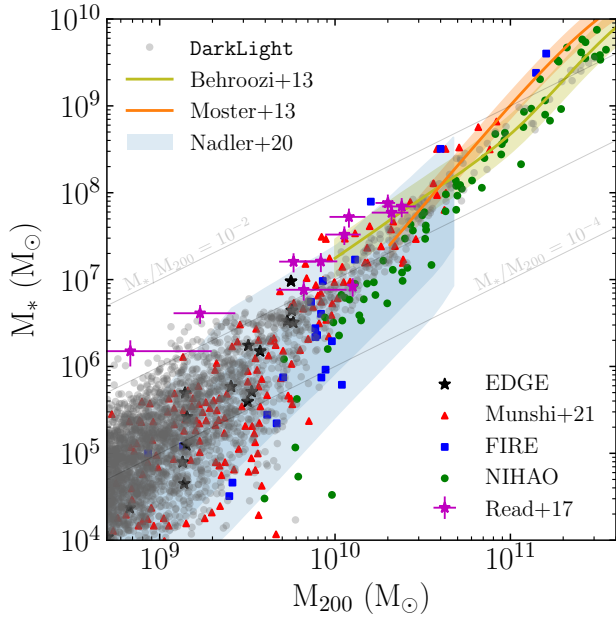


Figure 3. The SMHM relation predicted by DarkLight for haloes in EDGE’s parent void volume. DarkLight predictions are plotted in gray. Overplotted are dwarf galaxies from a variety of simulation studies, including EDGE (black stars; [Agertz et al. 2020](#); [Rey et al. 2020](#); [Orkney et al. 2021](#)), the DC Justice League and Marvelous Dwarf suites (red triangles; [Munshi et al. 2021](#)), FIRE (blue squares; [Chan et al. 2015](#); [Wheeler et al. 2015](#); [Wetzell et al. 2016](#); [Fitts et al. 2017](#)), and NIHAO (green circles; [Wang et al. 2015](#)). Observed gas-rich dwarfs from [Read et al. \(2017\)](#), which were used as part of the calibration data for DarkLight, are shown in magenta. These observed dwarfs are likely a biased subsample of low-mass dwarfs, representing the brightest members. At $M_{200} \gtrsim 10^{10} M_{\odot}$, DarkLight is in good agreement with abundance matching relations such as [Behroozi et al. \(2013\)](#) and [Moster et al. \(2013\)](#), which are plotted with yellow and orange lines, respectively.

tion transitions from star-forming dwarfs (including rejuvenators) to quenched reionisation relics (see Sec. 6). Thus if such a knee exists, the location of the knee, as well as the slopes above and below it, could point towards the timing of reionisation quenching, the mass scale at which dwarf galaxies rejuvenate, and differences in star formation rates before and after reionisation.

Finally, DarkLight naturally produces an increase in scatter towards smaller halo masses, as predicted by a number of hydrodynamic simulations (e.g. [Sawala et al. 2016](#); [Munshi et al. 2017](#)), galaxy-halo models ([Manwadkar & Kravtsov 2022](#); [O’Leary et al. 2023](#); [Ahvazi et al. 2024](#)), and explored in some abundance matching studies ([Garrison-Kimmel et al. 2017](#)) and fits to observed nearby dwarf galaxies ([Nadler et al. 2020](#); [Danieli et al. 2023](#)). The increase in scatter is often attributed to the rise in stochasticity of star formation at the low-mass end of galaxy formation. In contrast, DarkLight predicts that this scatter owes almost entirely to the combination of reionisation quenching and the scatter in the assembly histories of low mass dwarfs and is, therefore, deterministically predictable. We discuss this further in Section 4.1. The median relation predicted by DarkLight is given by:

$$\log M_* = 1.76 \log M_{200} - 10.7 \quad (3)$$

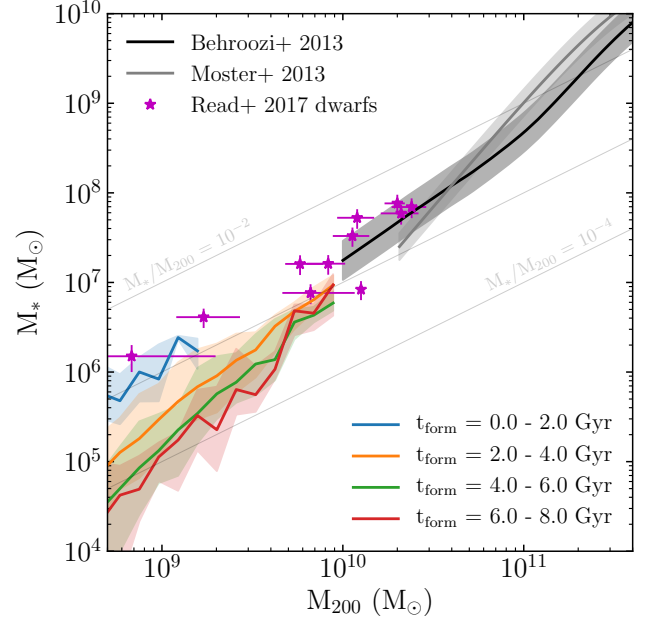


Figure 4. The SMHM relation predicted by DarkLight, broken down by halo formation time. Haloes have systematically higher stellar masses if they formed earlier for a fixed halo mass. The colored lines denote the median stellar masses for haloes with formation times t_{form} spanning from 0–8 Gyr. Formation times are defined as the time at which a halo achieves half of its present day mass. The shaded bands represent the 1σ scatter in M_* for the haloes in each t_{form} bin. There are no haloes with $t_{\text{form}} < 1.5$ Gyr above $\sim 10^9 M_{\odot}$, causing a truncation in this band.

with a increasing scatter described by:

$$\sigma = -0.227 \log M_{200} + 2.59 \quad (4)$$

At a halo mass of $10^9 M_{\odot}$, we measure a 1σ symmetric scatter in stellar mass of 0.49 dex. Similarly, [Nadler et al. \(2020\)](#) predict a similar though slightly larger scatter of ~ 0.56 dex (taking the average from the posterior) based on the Milky Way satellites. [Munshi et al. \(2021\)](#) predict a larger scatter of 0.73 dex, which could be due to their halo occupation fraction, which predict haloes with $M_{200} \gtrsim 10^9 M_{\odot}$ are occupied (see Sec. 4.2). These are significantly smaller than the 1.4 dex inferred by [Danieli et al. \(2023\)](#) when fitting an increasing scatter model to nearby dwarf satellite galaxies observed in the ELVES survey (although if they assume a constant scatter, they infer a very small scatter of 0.06 dex). This may be due to the additional quenching that dwarfs in their sample may experience as satellite galaxies, and/or the wide range of hosts their satellites are drawn from.

4.1 The origins and predictability of increasing scatter

The increase in scatter at the low-mass end is often attributed to an increase in the stochasticity of star formation in low-mass haloes. While the stochasticity of star formation does play a role, we find that, in the regime probed here, $M_{200} \gtrsim 10^9 M_{\odot}$, the majority of the SMHM scatter can instead be explained by the dark matter growth history of a low-mass halo—and is thus largely predictable.

Two distinct processes produce this increase in scatter. Firstly, the differences in the growth histories of dark matter haloes cause

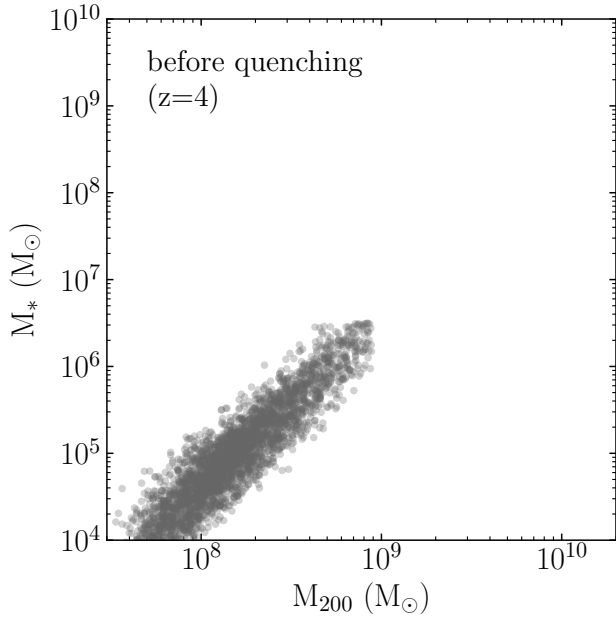


Figure 5. The SMHM at reionisation quenching ($z=4$) predicted by DarkLight for low-mass halos. Unlike DarkLight’s SMHM at $z = 0$, this does not exhibit an increase in scatter at low halo masses. The scatter at $< 10^9 M_\odot$ is roughly constant with a 1σ symmetric scatter of 0.23 dex. This demonstrates that the increasing scatter seen at $z = 0$ in low-mass haloes is due to post-reionisation evolution, namely that low mass dark matter haloes can grow in mass, while their stellar mass—quenched by reionisation—cannot (at least through in-situ star formation). The gray band denotes the numerical resolution limit for our simulations.

substantial scatter in the SMHM relation at the low mass end, as demonstrated for one EDGE halo that was “genetically modified” to grow faster or slower (Rey et al. 2019). We find that this holds true across the population of galaxies generated by DarkLight (we note that running on void halos may bias our sample towards later formation times). In Fig. 4, we show the median stellar masses for haloes with different formation times, which we define to be the time when a halo reaches half of its present-day mass. The difference between the medians of the lowest and highest formation time bins is about an order of magnitude at $10^9 M_\odot$, in agreement with Rey et al. (2019), and decreases at higher masses. Below $M_{200} \lesssim 10^{10} M_\odot$, we find that for a fixed halo mass, the earliest forming haloes tend to host the most massive galaxies, while the latest forming haloes host the least massive galaxies. This implies that early formers tend to sit in the upper envelope of the SMHM relation, while later formers sit in the lower envelope. For many of these galaxies, the vast majority of their stellar mass formed before reionisation. Their haloes assembled a greater fraction of their final mass by reionisation (and thus have a higher pre-reionisation v_{\max}) and thus were able to form stars at a higher rate before being quenched.

Secondly, after reionisation, low-mass haloes halt star formation until they are sufficiently massive (as captured by our threshold $v_{\max}^{\text{post}} = 26.3 \text{ km/s}$ in DarkLight). Thus, while before reionisation, the dark matter and stellar masses could grow roughly in step with one another, reionisation decouples the two. Stellar masses can remain largely stagnant after reionisation, while their dark matter haloes can continue to grow. As the growth in dark matter mass can vary for

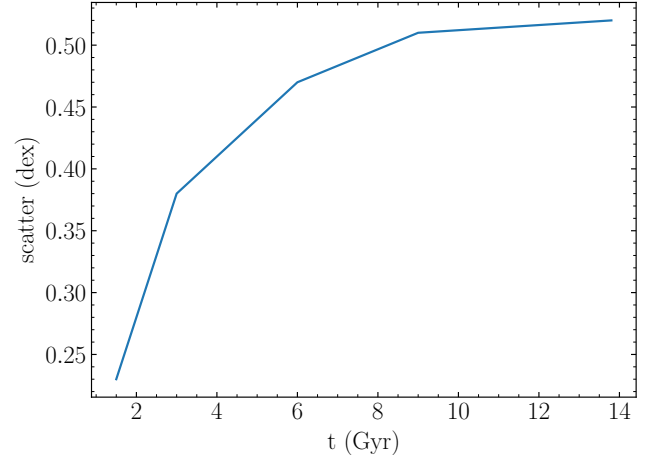


Figure 6. Growth in the SMHM scatter for progenitors of $M_{200}(z = 0) = 10^9 M_\odot$ haloes over time. At reionisation quenching, which occurs at $\sim 1.5 \text{ Gyr}$ in EDGE and DarkLight, there is a constant 1σ scatter of about 0.23 dex, which grows to about 0.5 dex by the present day.

different haloes, this produces an increase in SMHM scatter over time. In Fig. 5, we show the SMHM predicted by DarkLight when reionisation quenching occurs ($z \sim 4$ in EDGE). Unlike the SMHM at $z = 0$, the scatter is roughly constant at the low-mass end. We measure a 1σ scatter of about 0.23 dex in the progenitors of haloes with a $z = 0$ mass of $10^9 M_\odot$. Notably, this is similar to the size of the SMHM scatter observed at $z = 0$ for massive, star-forming galaxies. This grows to a scatter of 0.5 dex by $z = 0$. In Fig. 6, we show how the scatter for progenitors of $M_{200}(z = 0) = 10^9 M_\odot$ haloes increases over time. We have confirmed that scatter also grows over time following reionisation for low-mass haloes in the galaxy formation model GALACTICUS (Ahvazi, private communication).

Lastly, the fact that scatter is not uniform at the low-mass end, but increases with decreasing halo mass is due to the decreasing star formation efficiency of low-mass haloes. In other words, after reionisation, the most massive quenched dwarfs can continue growing in stellar mass through the accretion of smaller galaxies, allowing them to evolve close to the pre-reionisation SMHM track. However, quenched galaxies of lower mass accrete a higher fraction of dark, starless subhaloes, causing them to grow relatively more in their dark versus luminous mass.

Together, the above results imply that the stellar masses of individual haloes and the scatter in the SMHM relation is predictable if the accretion histories of haloes are known. *The stochasticity of star formation is not the main driver of the SMHM scatter* at least down to halo masses of $\sim 10^9 M_\odot$.

4.2 Impact of uncertainties in the physics of reionisation quenching

The interplay of reionisation and halo growth histories in shaping the scatter in the SMHM underscores the key role that the physics of reionisation quenching plays in shaping the SMHM relation, including its shape, slope, and normalisation. In Figure 7, we show how sensitive the location, slope, and scatter in the SMHM relation is to changes in DarkLight’s reionisation quenching model. In all panels, the fiducial relation predicted by DarkLight is plotted in black.

In the leftmost panel, we show the impact of the timing of reionisa-

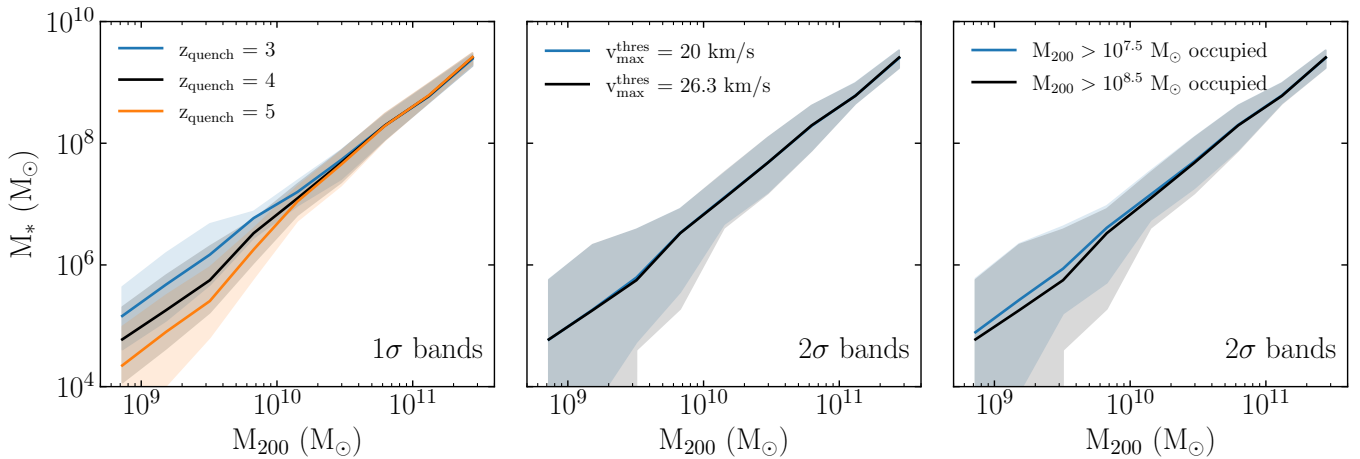


Figure 7. Impact of uncertainties in the physics of reionisation quenching on the scatter, slope, and shape of the SMHM relation. In all panels, the fiducial model is shown in black. (*Left*) The timing of reionisation quenching affects the shape, slope, and scatter of the SMHM relation at the low-mass end. Earlier quenching at $z_{\text{quench}} = 5$ (orange) results in scatter larger by 0.6 dex, a steepening of the relation at the low-mass end, and the presence of a “knee”. The bands represent the 1σ scatter. Later quenching at $z_{\text{quench}} = 3$ (blue) produces smaller scatter and a single power law with no knee. (*Middle*) The threshold $v_{\text{max}}^{\text{post}}$ required for haloes to reach in order for quenched galaxies to resume star formation after reionisation mildly affects the scatter in the SMHM relation. Decreasing $v_{\text{max}}^{\text{post}}$ from 26.3 km/s (fiducial; black) to 20 km/s (blue) so that more lower-mass haloes rejuvenate mildly reduces the scatter in the SMHM relation, but does not affect the slope or shape of the relation. Increasing the threshold does not change the scatter. (*Right*) Increasing the occupation fraction such that 50% of haloes with masses of $10^{8.5} M_{\odot}$ instead of $10^{7.5} M_{\odot}$ are occupied reduces the steepness of the slope and the scatter in the SMHM relation. The 1σ scatter is reduced by ~ 0.1 dex.

tion quenching, z_{quench} . As expected, later quenching at $z_{\text{quench}} = 3$ (blue) allows for low-mass haloes to form stars for a longer period of time, elevating the SMHM relation. While our fiducial model shows signs of a slight steepening in slope for $M_{200} \lesssim 10^{10} M_{\odot}$, later quenching produces an unbroken power law. We find that if we adopt an earlier quenching redshift, $z_{\text{quench}} = 5$ (orange), *DarkLight* similarly predicts a stronger knee in the SMHM relation. Across the range of quenching redshifts we explored, we find the SMHM slope systematically steepens from $a_{\text{SMHM}} = 1.57$ for $z_{\text{quench}} = 3$ to $a_{\text{SMHM}} = 1.91$ for $z_{\text{quench}} = 5$. The scatter at the low-mass end becomes systematically larger with earlier quenching, which increases the fraction of haloes accreted by low-mass galaxies that are devoid of stars. At a halo mass of $10^9 M_{\odot}$, the 1σ scatter increases to ~ 0.61 dex when we adopt an earlier quenching of $z_{\text{quench}} = 5$. Conversely, if quenching occurs later, at $z_{\text{quench}} = 3$, the scatter decreases to 0.50 dex. Given that reionisation is believed to occur inhomogeneously (Aubert et al. 2018; Keating et al. 2020; Ocvirk et al. 2020; Katz et al. 2020, e.g.), and that denser regions likely reionise first, this implies that the SMHM may exhibit differences with environment (Christensen et al. 2024).

The lower envelope of the SMHM relation is affected by the chosen rejuvenation threshold, i.e. the threshold required for quenched galaxies to resume forming stars. In *DarkLight*, we adopt a fiducial value of $v_{\text{max}}^{\text{post}} = 26.3$ km/s, which best fits the hydrodynamic simulations of the EDGE dwarf galaxies. In the middle column of Fig. 7, we show how the SMHM changes when we adopt $v_{\text{max}}^{\text{post}} = 20$ km/s in blue. The shaded bands represent the size of the 2σ scatter. The lower threshold allows more galaxies, particularly those in low-mass haloes, to rejuvenate. We see this raise the lower envelope of the SMHM relation $\lesssim 10^{10} M_{\odot}$, decreasing the scatter in the SMHM relation. We find that increasing the threshold to 30 km/s does not change the SMHM nor its scatter.

Another significant uncertainty that affects the evolution of the SMHM after reionisation is the fraction of haloes that are expected

Table 1. Functional fits for SMHM with varied input parameters

variant	a_{SMHM}	b_{SMHM}	a_{scatter}	b_{scatter}
fiducial	1.76	-10.7	-0.227	2.59
poccALL	1.72	-10.3	-0.194	2.22
poccN18	1.73	-10.4	-0.202	2.3
$v_{\text{max}}^{\text{post}} = 20$ km/s	1.76	-10.8	-0.235	2.66
$v_{\text{max}}^{\text{post}} = 30$ km/s	1.75	-10.7	-0.224	2.56
$z_{\text{quench}} = 3$	1.57	-8.71	-0.217	2.45
$z_{\text{quench}} = 5$	1.91	-12.4	-0.24	2.77

to host a galaxy as a function of halo mass, i.e. the occupation function. Given the role that dark subhaloes play in increasing the size of the scatter in the SMHM (see Sec. 4.1), one expects that if a larger fraction of low-mass haloes host galaxies, the smaller the growth in scatter at the low-mass end will be. We find this to be true with *DarkLight*. In the rightmost panel of Fig. 7, we show that if we adopt an occupation function such that 50% of halos with masses of $M_{200} > 10^{8.5} M_{\odot}$ host galaxies, we obtain the relation in black. The shaded bands represent the 2σ scatter in the relation. If instead, we shift the occupation function towards lower masses so that 50% of halos with masses of $10^{7.5} M_{\odot}$ host galaxies, we find that the SMHM shifts upwards, as does the bottom of the 2σ scatter envelope. The latter threshold is favored by Nadler et al. (2020), who inferred from the Milky Way dwarfs that nearly all haloes down to $10^8 M_{\odot}$ host galaxies (see also Sec. 5 and Fig. 8). At a halo mass of $10^9 M_{\odot}$, this reduces the 1σ scatter by 0.07 dex, from 0.55 dex to 0.48 dex.

In Table 1, we show how the functional fit to the median and scatter in the SMHM changes for each of the models we explored.

5 THE HALO OCCUPATION FRACTION

DarkLight also predicts which haloes host galaxies, and which should stay completely dark, i.e. the halo occupation fraction. In

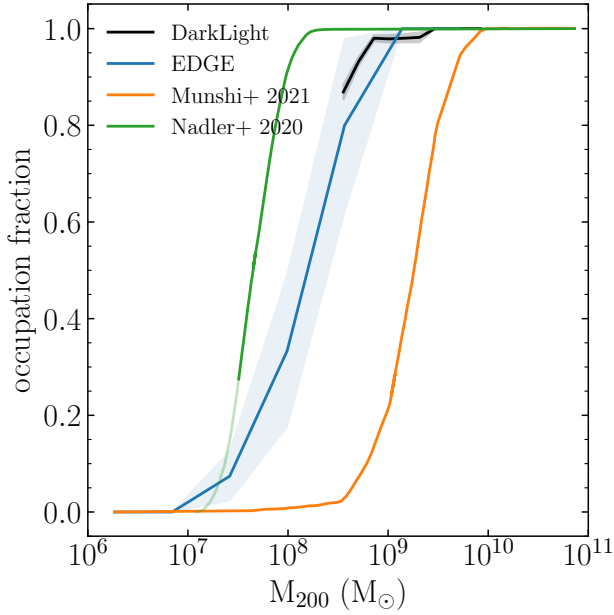


Figure 8. The halo occupation fraction predicted by DarkLight (black), shown down to the resolution limit of the void volume on which it was run (corresponding to a halo mass limit of $\sim 3 \times 10^8 M_\odot$). This is compared to that from the EDGE hydrodynamic zoom simulations (blue), the Marvel-ous Dwarfs and DC Justice League suites (Munshi et al. 2021) (orange; based on their sample of galaxies with >1 star particle), and inferred from fitting the Milky Way satellite luminosity function by (Nadler et al. 2020) (green). The latter is shown in light green at the mass scales below the resolution limit of the simulations based on which the fit was performed.

Fig. 8, we show DarkLight’s prediction in black. The results are in good agreement with the EDGE simulations, which are shown in blue (bands denote statistical uncertainties), and includes all haloes that have at least one star particle (which are initialized with a mass of $300 M_\odot$, but can undergo mass loss due to supernovae and winds from massive stars). Due to the resolution of the void volume on which DarkLight was run, we do not have reliable statistics on the occupation fraction of haloes below $M_{200} \sim 3 \times 10^8 M_\odot$ (in contrast, the galaxies in the EDGE suite are zooms that go to much higher resolution). We expect that due to limited numerical resolution, the results from the EDGE simulations are a *lower bound* on the fraction of haloes that host galaxies. We also show the results from the Marvel-ous Dwarfs and DC Justice League simulations (Munshi et al. 2021), again showing all haloes with at least one star particle, and from a fit to observed Milky Way satellite galaxies (Nadler et al. 2020). DarkLight and EDGE predict haloes are occupied to lower halo masses than in Munshi et al. (2021), but higher halo masses than inferred by Nadler et al. (2020). Munshi et al. (2021) show that the occupation fraction inferred is strongly dependent on resolution, and thus the mismatch between Nadler et al. (2020) versus that from DarkLight and both simulation suites could be due to issues in resolution.

6 STAR-FORMING VERSUS QUENCHED DWARFS

The presence of star-forming (or recently star-forming) dwarf galaxies with very low stellar masses has been an enduring puzzle. These

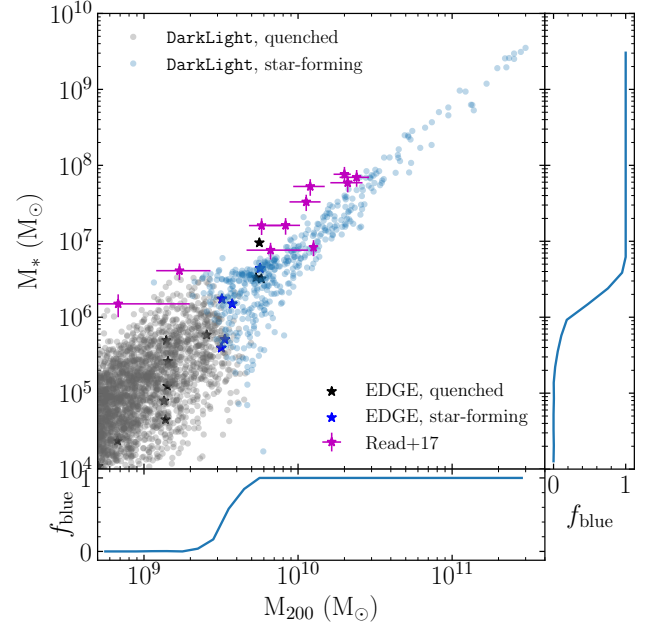


Figure 9. Distribution of star-forming and quenched dwarf galaxies predicted by DarkLight. The points and symbols are as in 3, but with galaxies shaded blue if they are identified to be star-forming today, which we take to be haloes with $v_{\max}(z=0) > v_{\max}^{\text{post}} = 26.3$ km/s, or shaded gray if they are quenched. Similarly, dwarfs in the EDGE simulations suite (stars) are shaded blue if they are star-forming at the present day. Observed gas-rich, star forming, galaxies are plotted in magenta (Read et al. 2017). The bottom and right panels show the fraction of dwarfs that are star-forming today, as a function of halo or stellar mass, respectively. There is a sharp transition from quenched to star-forming at halo masses of a few $10^9 M_\odot$, and stellar masses of a few $10^6 M_\odot$. DarkLight currently does not model self-quenching due to starbursts, which have been observed in some EDGE dwarfs (black stars at $M_{200} \sim 10^{10} M_\odot$; Gray et al. 2024). As such, the transition between quenched and star-forming galaxies may not be quite as steep once these are factored in, and the boundary we find between them should be taken as a theoretical lower bound.

include galaxies such as Aquarius, CVndwIa, Leo T, Leo P, Antila B, and Peg W, which have stellar masses as low as $\sim 10^5 M_\odot$, and are thought to inhabit haloes of mass less than $\sim 5 \times 10^9 M_\odot$ (Read et al. 2017; Zoutendijk et al. 2021). While recent high-resolution simulations (Wright et al. 2019; Rey et al. 2020; Applebaum et al. 2021; Gutcke et al. 2022) and some semi-empirical models (Benitez-Llambay & Fumagalli 2021; O’Leary et al. 2023; Ahvazi et al. 2024) have begun to reproduce analogs of galaxies like Leo T, including their HI content (Rey et al. 2022), dwarfs such as Aquarius and CVndwIa, that have high stellar mass at such low halo mass, remain a challenge to reproduce.

As DarkLight produces star formation histories, it can identify which haloes are likely star-forming or quenched today. We can thus search for analogs of low-mass, star-forming dwarfs. In Fig. 9, we plot galaxies predicted by DarkLight, but shade in light blue those haloes predicted to be star-forming today (i.e. $v_{\max}(z=0) > 23.5$ km/s). We find that haloes with $M_{200} \gtrsim 5 \times 10^9 M_\odot$ are all star-forming. Below this mass, some haloes without ongoing star formation begin to appear, increasing in number until $M_{200} \lesssim 2 \times 10^9 M_\odot$, below which all haloes are quenched. This agrees with the threshold found in other theoretical work (Christensen et al. 2024). The fraction of haloes that are star-forming as a function of halo mass is shown in

the bottom panel. We find that 50% of dwarfs are star-forming at a halo mass of $\sim 4 \times 10^9 M_\odot$.

In terms of stellar mass, all galaxies are star forming down to $M_* \sim 5 \times 10^6 M_\odot$, at which point quiescent dwarfs begin to appear. The fraction of galaxies that are star-forming as a function of stellar mass is shown in the right panel. About 50% of dwarfs are star-forming at $M_* \sim 2 \times 10^6 M_\odot$. There is a small but significant tail of star-forming galaxies with $M_* \lesssim 10^6 M_\odot$.

We note that DarkLight does not include self-quenching of dwarfs due to starbursts, and thus some dwarfs that we predict to be star-forming may be quenched (e.g. black stars at $M_{200} \sim 10^{10} M_\odot$ in Fig. 9; and see also Gray et al. 2024). The mass thresholds above can thus be considered as *lower limits* on the mass scale at which dwarf galaxies are star forming. Further, the transition between star-forming and quiescent dwarfs may not be quite as steep as we predict.

With this in mind, we find that DarkLight predicts star-forming analogs of Aquarius and CVndwIa, which are represented by the two leftmost magenta data points, respectively. The haloes that correspond to these particularly low-mass dwarf irregulars tend to be early formers that assembled their stellar content early, then resumed forming stars only in the last few billion years. Although they are rare, DarkLight also predicts analogs for dwarfs with even lower stellar masses such as Leo T, Leo P, Antila B, and Peg W. In contrast to Aquarius, these low stellar mass dwarfs tend to be late formers that have undergone recent mass growth. A detailed comparison of predictions by DarkLight to observational measurements of the star formation histories and kinematics of these low-mass galaxies will be presented in future work. These lowest-mass star-forming galaxies are the tip of the iceberg of a much larger population of quiescent galaxies at this mass scale. Indeed, a quenched field dwarf that may be consistent with reionisation quenching has recently been discovered (Hedgehog, Li et al. 2024). Such galaxies represent highly valuable constraints on galaxy formation models, which must reproduce these systems. We will further test this in future work by simulating these low-mass star-forming analogs with full hydrodynamics.

6.1 Impact of uncertainties in the physics of reionisation quenching

Here, we show how sensitive the boundary between star-forming dwarfs and reionisation relics is to uncertainties in the physics of reionisation quenching. In the left panel of Fig. 10, we show how changes in the threshold v_{\max} required to for galaxies quenched by reionisation to reach to resume star formation affects the boundary. As expected, lowering the threshold lowers the (halo and stellar) mass of the boundary between star-forming dwarfs and reionisation relics, and vice versa. Lowering the threshold from the fiducial value of $v_{\max}^{\text{post}} = 23.5$ km/s to 20 km/s has a dramatically larger effect than increasing it to 30 km/s. A threshold of 20 km/s lowers the stellar mass at which 50% of galaxies are star-forming by nearly an order of magnitude to $3 \times 10^5 M_\odot$, compared to the fiducial value of $2 \times 10^6 M_\odot$, while increasing it to 30 km/s raises it to $3 \times 10^6 M_\odot$. In terms of halo mass, a threshold of 20 km/s lowers the 50% point to $10^9 M_\odot$, compared to the fiducial value of $4 \times 10^9 M_\odot$, while increasing the threshold to 30 km/s raises it to $5 \times 10^9 M_\odot$.

In the right panel of Fig. 10, we change the redshift at which dwarf galaxies quench. This does not alter the halo mass of the boundary between star-forming and quenched dwarfs. However, as earlier quenching truncates stellar mass growth earlier, their stellar masses are lower than if quenching occurred later. This shifts the boundary between star formers and quenched dwarfs to lower stellar

masses. For a quenching redshift $z_{\text{quench}} = 5$, the stellar mass at which 50% of galaxies are star-forming shifts to $M_* = 7 \times 10^5 M_\odot$, from the fiducial value of $2 \times 10^6 M_\odot$, while later quenching at $z_{\text{quench}} = 3$ shifts the threshold to $4 \times 10^6 M_\odot$.

7 DISCUSSION

7.1 Comparison with other galaxy formation models

Below scales of $\sim 10^{10} M_\odot$, there are a handful of galaxy formation models tailored to model dwarf galaxies. Those calibrated on higher-mass galaxies do not necessarily work at low-mass scales, in part due to the lack of reionisation quenching and its impact on galaxy growth. Those that do exist adopt different approaches to modelling dwarf evolution, ranging from UNIVERSEMACHINE (Behroozi et al. 2019) and EMERGE (Moster et al. 2018), semi-empirical models constrained by observations, GRUMPY, a regulator model that models gas inflow, outflow, and star formation (Kravtsov & Manwadkar 2022), Galacticus and GALFORM, fully semi-analytic codes (Benson 2012; Cole et al. 1994), and SatGen, an emulator based on numerical simulations (Jiang et al. 2021).

7.1.1 UNIVERSEMACHINE

DarkLight’s reliance on empirical relations to calibrate the dependence of star formation rates on v_{\max} is most similar to UNIVERSEMACHINE (Behroozi et al. 2019). However, they differ in two important regards. Firstly, DarkLight is calibrated on observations where available, and supplemented by high-resolution simulations where they run out, and is thus calibrated to $M_{200} \sim 10^9 M_\odot$, corresponding to a median $M_* \sim 10^5 M_\odot$. In contrast, UNIVERSEMACHINE is exclusively fit to observations. While DarkLight fits mean SFRs to fit two $\langle \text{SFR} \rangle$ - v_{\max} relations, UNIVERSEMACHINE performs a MCMC fit for the instantaneous SFR as a function of redshift using a wide array of observations concerning massive galaxies, including stellar mass and UV luminosity functions, specific and cosmic SFRs, and quenched fraction, among others. Recently, it was recalibrated with data from the SAGA survey of satellites around MW analogues, which is largely complete down to dwarfs with $M_* \gtrsim 10^{7.5} M_\odot$ (Mao et al. 2024), and isolated SDSS field galaxies down to $M_* \gtrsim 10^7 M_\odot$, extending its calibration range (Wang et al. 2024). Although DarkLight is calibrated down to much lower mass scales, its dependence on hydrodynamic simulations for $v_{\max} \lesssim 20$ km/s implies that our results at the low-mass end are dependent on the subgrid physics adopted in EDGE. However, the EDGE simulations match observed dwarfs well (e.g. Agertz et al. 2020; Richstein et al. 2024).

A second important difference is that we model reionisation, while UNIVERSEMACHINE does not. This causes UNIVERSEMACHINE to predict too many star-forming dwarf galaxies (Wang et al. 2021, although this has improved with the addition of environmental quenching, c.f. Wang et al. 2024). DarkLight predicts a more realistic distribution of star-forming and quenched dwarfs (c.f. Sec 6). Despite these differences, DarkLight and UNIVERSEMACHINE produce similar SMHMs, as shown in Fig. 11, albeit systematically lower in stellar mass by about a factor of 2-3, and reproduces the SMHM inferred from the MW dwarfs (Nadler et al. 2020) well. As Wang et al. (2021) predicted, UNIVERSEMACHINE produces realistic stellar masses as the suppression of star formation due to reionisation quenching is made up for by enhanced SFRs before reionisation, which is observed

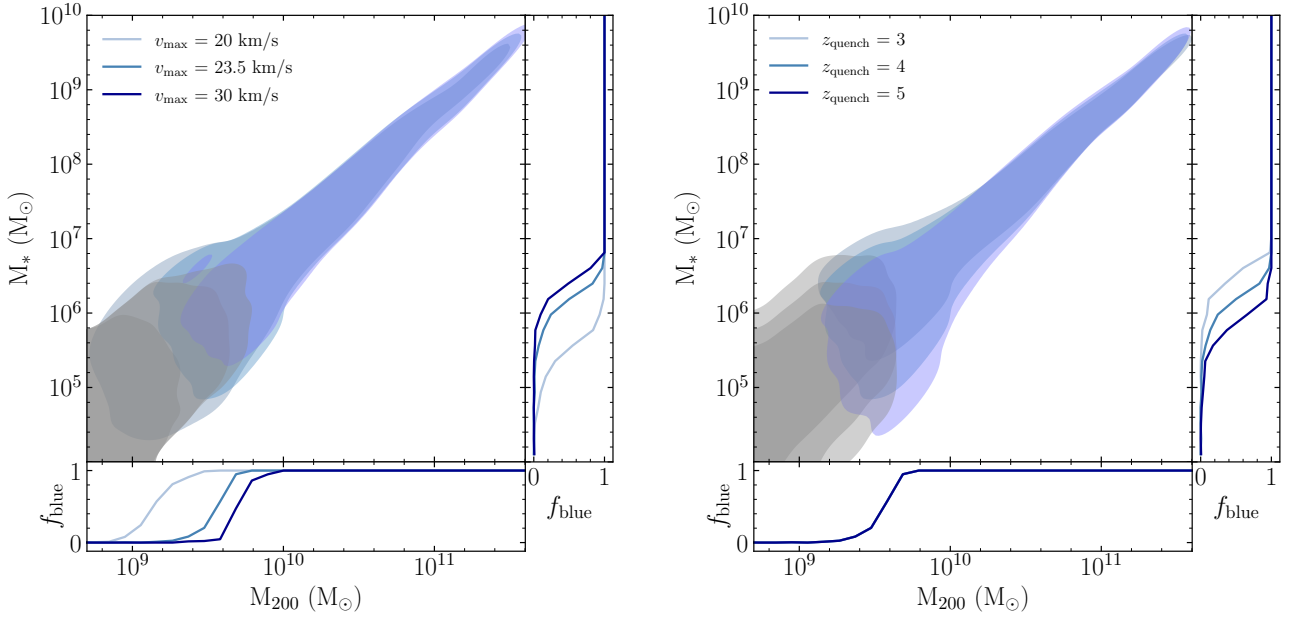


Figure 10. Change in the distribution of star-forming (blue) versus quenched (gray) dwarf galaxies due to modifications to DarkLight’s input physics. *Left:* Lowering (raising) the threshold needed for dwarf galaxies quenched by reionisation to rejuvenate shifts the boundary between star-forming dwarfs and reionisation relics to lower (higher) masses. *Right:* If galaxies quench earlier (later), they form fewer (more) stars, pushing the boundary between star-formers and reionisation relics to lower (higher) stellar masses. The boundary in halo mass remains unchanged.

in the EDGE simulations. However, as they do not include reionisation quenching, the SMHM relation predicted by UNIVERSEMACHINE does not exhibit an increase in scatter at low masses.

Lastly, we note that we have calibrated on isolated dwarfs, while UNIVERSEMACHINE includes environmental physics (Wang et al. 2024). We will add environmental physics in future work.

7.1.2 EMERGE

EMERGE is also based on a wide range of empirical relations, initially primarily of massive galaxies (Moster et al. 2018). However, instead of relying on a relation between SFR and v_{\max} , EMERGE scales SFRs based on the change in mass of a dark matter halo over time. This assumes that accreted gas can be converted into stars within a dynamical time. This assumption breaks down at dwarf scales due to reionisation quenching. EMERGE was recently updated to include reionisation quenching, fitting to a stellar mass function extended to include observed Local Group dwarfs with $M_* \gtrsim 10^5 M_\odot$ to infer the threshold mass below which galaxies were quenched (O’Leary et al. 2023). Their preferred model for comparison (‘logistic’, see their Fig. 2) quenches dwarfs around $z \sim 4$ with masses $M_{\text{halo}} \lesssim 2 \times 10^9 M_\odot$ (note that while they explored the redshift dependence of the mass cutoff, they did not find it was strongly constrained by the data). In contrast, DarkLight identifies quenched galaxies as those with $v_{\max} < 26.3$ km/s at $z_{\text{quench}} = 4$, which corresponds to a similar cutoff halo mass as in EMERGE. In Fig. 11, we show the SMHM of EMERGE for their model with reionisation quenching in green. Unlike the other SMHM relations, the median and scatter were reported for galaxies binned in stellar mass, rather than halo mass. With this in mind, we find that the median relation predicts stellar masses an order of magnitude lower than DarkLight. We note that their reference model (not plotted), which does not include reionisation quenching, produces a SMHM relation and scatter more consistent with,

though still systematically lower than, that predicted by DarkLight and other galaxy-halo models.

7.1.3 GRUMPY

GRUMPY is a galaxy formation code tailored to dwarf galaxies that distills key galaxy formation physics into a few differential equations that describe gas inflow, outflow, and sinks—an approach described as a “regulator” or “bathtub” model (e.g. Peng et al. 2010). Like EMERGE, they tie gas inflow rates to the dark matter accretion rate, which are derived from dark matter only simulations. However, they include more detailed modeling of reionisation quenching, H_2 cooling, and galactic outflows, among others (Kravtsov & Manwadkar 2022). GRUMPY’s prediction for the SMHM relation, based on forward-modelling the MW satellites (Manwadkar & Kravtsov 2022), is shown in red in Fig. 11. This favors a broad range of reionisation redshifts spanning $z \sim 7 - 10$. Like DarkLight, they also find an increase in scatter at halo masses below $10^{10} M_\odot$. Kravtsov & Manwadkar (2022) find that adopting earlier reionisation results in a similar steepening in the slope at the low-mass end. They also find that the SMHM relation is sensitive to the wind model they adopt. We note that the EDGE simulations upon which DarkLight is based self-consistently resolves momentum and energy injection by individual supernovae, but does not include a model for radiative transfer. The latter acts to suppress strong outflows in the lowest mass dwarfs (Agertz et al. 2020), lowering the stellar mass for a given halo mass.

7.1.4 Semi-analytic models: Galacticus

Semi-analytic codes include detailed models of the many physical processes involved in galaxy formation. While a number of semi-analytic codes exist, Galacticus in particular has recently been

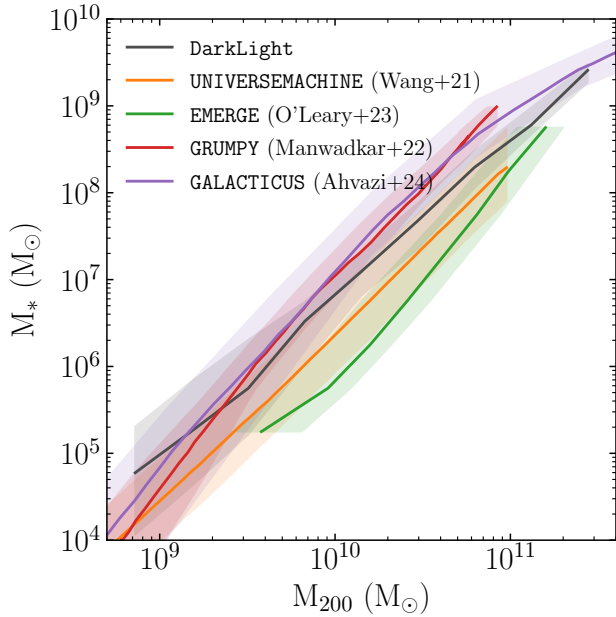


Figure 11. SMHMs predicted by various galaxy formation models. Bands denote 1σ contours. DarkLight, UNIVERSEMACHINE (Wang et al. 2021), and EMERGE (O’Leary et al. 2023) are semi-empirical models, GRUMPY (Manwadkar & Kravtsov 2022) is a regulator model, and GALACTICUS (Ahvazi et al. 2024) is a fully semi-analytic model. UNIVERSEMACHINE currently does not include reionisation. For EMERGE, the SMHM based on the “High- z quench” reionisation model is shown. Note that the contours for EMERGE denote the scatter in halo mass for a given stellar mass bin rather than the scatter in stellar mass for a given halo mass, in contrast to the other relations. UNIVERSEMACHINE and SatGen do not model reionisation.

extended to dwarf scales by Ahvazi et al. (2024). They include an updated UV background model for reionisation (favoring a reionisation redshift of $z = 7.8$), a new model for the metallicity of the intergalactic medium and, crucially, H_2 cooling, which they find is required to match the mass-metallicity relation and the inferred halo occupation function of the MW satellites. GALACTICUS’s predictions for the SMHM is shown in Fig. 11 in purple. It closely matches the prediction by DarkLight and exhibits an increase in scatter at the low mass end that similarly grows following reionisation quenching (Ahavazi, private comm.). It exhibits a steepening of the SMHM slope at slightly higher halo masses of $\sim 10^{11} M_\odot$ than in other work (e.g. Munshi et al. 2021).

While GALFORM, another semi-analytic code, has also been used in studies of dwarf galaxies, including to study the impact of reionisation on the luminosity function at the faint end (e.g. Bose et al. 2018), their predictions for the SMHM relation have not been published, so we do not discuss this model in detail here.

7.1.5 SatGen and other models that sample from a SMHM relation

While the models discussed above *predict* the SMHM relation from various assumptions on how to model galaxy formation, many dwarf galaxy studies simply adopt a published SMHM relation and sample stellar masses from its scatter. Of note, this is the approach taken by SatGen (Jiang et al. 2021), an emulator based on numerical simulations that tracks in detail the evolution of satellites in a host halo.

SatGen utilises a SMHM relation derived via abundance matching by Rodríguez-Puebla et al. (2017), which is calibrated for haloes with present-day masses $M_{\text{vir}} \gtrsim 10^{10} M_\odot$, and thus relies on extrapolations to dwarf galaxies below this mass (i.e. likely for most of the ultrafaint dwarf galaxies). Notably, it adopts a constant scatter of 0.16 dex, and thus does not include the impact of reionisation on the shape, slope, normalisation, or scatter in the SMHM relation. Further, we note that studies that similarly assign haloes a stellar mass by simply sampling from the scatter of a SMHM relation will miss the dependence of stellar masses on dark matter accretion histories.

7.2 Comparison with simulations

In light of the sensitivity of the SMHM relation to the halo occupation function and uncertainties in the physics of reionisation quenching, it is not surprising that hydrodynamic simulations differ in their predictions for the SMHM by as much as two orders of magnitude below halo masses of $\sim 10^{10} M_\odot$ (see Fig. 3 and Garrison-Kimmel et al. 2017). These physics are highly uncertain in simulations of dwarf galaxies.

Resolution is important to avoid numerical quenching due to poorly resolved gas content and star formation in low-mass dwarf galaxies. Munshi et al. (2021) showed that the halo occupation function can shift by an order of magnitude depending on one’s resolution. Recent simulations have begun to achieve sufficient resolution to resolve $\lesssim 10^{10} M_\odot$ haloes. Resolution studies performed by some groups running very high-resolution hydrodynamic simulations show that stellar masses of $10^9 M_\odot$ haloes remain largely unchanged with increased resolution (e.g. Munshi et al. 2021), while others find that increasing their dark matter resolution by a factor of ~ 10 caused their stellar masses to increase by a factor of 2 (Agertz et al. 2020). There are still significant differences between these simulation suites, underscoring that resolution cannot explain the entirety of the differences between hydrodynamic simulations.

The remaining discrepancies likely owe in large part to differing subgrid physics governing star formation and evolution. Importantly, supernovae feedback models are highly uncertain yet are key to determining stellar masses of dwarf galaxies. Agertz et al. (2020) showed that a given halo can form more than an order of magnitude more stars if it has weak or no feedback; radiative transfer can further reduce the stellar mass by another order of magnitude. Non-equilibrium cooling can then counteract this by allowing more stars to form (Rey et al. in prep 2024). Munshi et al. (2019) showed that using a classical temperature-density threshold for star formation produced more dwarf galaxies than using a non-equilibrium H_2 -cooling threshold. Furthermore, few simulations model cosmic ray feedback and magnetic fields, which affect the stellar mass of dwarf galaxies in non-linear ways (e.g. Hopkins et al. 2020; Martín-Alvarez et al. 2023). However, subgrid physics is not the only driver of differences in stellar masses. Hu et al. (2023) showed that Eulerian and Lagrangian codes—all sub-grid physics being as equal as possible—can produce significant differences in the burstiness of star formation, which can impact the stellar mass they form.

The fact that simulations begin to differ at $10^{10} M_\odot$ is perhaps key to note. This is the scale at which reionisation relics begin to dominate the population (e.g. §6). Thus the stellar content of these haloes will largely (if not entirely) be set by the physics of reionisation and of galaxy formation in the early universe. Benitez-Llambay & Frenk (2020) showed that both can shift the halo occupation function by orders of magnitude. Further complicating matters, reionisation is believed to be inhomogeneous, with dense environments reionising earlier than low-density regions (Aubert et al. 2018; Keating et al.

2020; Ocvirk et al. 2020; Katz et al. 2020, e.g.), implying that the SMHM and its scatter should vary with environment (as shown by Christensen et al. 2024). H_2 cooling appears to be an essential ingredient to reproduce reionisation relics around the MW (Manwadkar & Kravtsov 2022; Ahvazi et al. 2024). Reducing uncertainties on the reionisation models and the subgrid physics that governs the formation of dwarf galaxies before reionisation will be key to understanding the true form of the SMHM.

7.3 Limitations of DarkLight

In this section, we briefly highlight a few current known caveats and limitations of DarkLight and discuss where and how these can be addressed in future work.

- (i) **Episodic star formation:** DarkLight assumes a *mean* star formation rate whenever haloes are identified to be actively forming stars and does not model stochasticity. However, observed star forming dwarf irregulars (Collins & Read 2022), as well as EDGE dwarfs that become sufficiently massive to reignite star formation after reionisation, exhibit episodic star formation (Fig. 2). We will explore adding periodicity and/or stochasticity to the mean star formation rates in DarkLight, which can be calibrated both by simulations like EDGE, or empirically fit to the latest data constraints (e.g. Collins & Read 2022).
- (ii) **Starbursts and self-quenching:** DarkLight can produce a temporary burst of star formation in dwarfs quenched by reionisation due to mergers (e.g. Halo 600 in Fig. 2) caused by temporary rises in v_{\max} that accompany mergers, if it passes above the rejuvenation threshold. However, in EDGE, we find that such mergers can excite starbursts with star formation rates significantly higher than given by our $\langle \text{SFR} \rangle - v_{\max}$ relation, with the feedback from such events being sufficient to fully self-quench the dwarf (Gray et al. 2024). We will explore adding such a starburst model to DarkLight in future work (Gray et al., in prep).
- (iii) **Calibration on EDGE:** For low mass dwarfs, DarkLight is currently calibrated on the EDGE simulation suite, and thus its predictions are as accurate insofar as these simulations are a reliable facimile of nature. As discussed in Sec. 7.2, switching to an alternative cosmological code and/or different subgrid model choices could yield significant changes. DarkLight can be calibrated on other simulations, and ultimately be calibrated fully on data, if data of sufficient quality become available for galaxies with $v_{\max} < 20$ km/s. We are exploring how changes in subgrid physics in the EDGE2 suite (Muni et al. 2024, Rey et al, in prep.) modify our predictions for the SMHM relation.

8 CONCLUSIONS

We have presented a new semi-empirical code, DarkLight, designed to predict the stellar mass assembly history of dwarf galaxies, down to the very faintest systems. We found that the interplay between reionisation and halo growth histories is key to determining the slope, scatter, and shape of the stellar-mass–halo-mass (SMHM) relation. Our main conclusions are as follows:

- For higher-mass dwarfs with $M_{200} \gtrsim 10^{10} M_{\odot}$, DarkLight’s prediction for the SMHM relation agrees well with abundance matching, simulations, and observational studies. Below this scale, where studies differ significantly, DarkLight predicts a large scatter, with a 1σ symmetric scatter at $M_{200} = 10^9 M_{\odot}$ of 0.5 dex.

- The scatter in the SMHM relation down to $M_{200} \lesssim 10^9 M_{\odot}$ is not predominantly due to stochastic star formation. Instead, the truncation of galaxy growth due to reionisation, which decouples the growth of the stellar mass from the halo mass of a galaxy, combined with the wide range of halo assembly histories, accounts for the majority of the scatter.
- The scatter in the SMHM is constant for low-mass haloes at reionisation, but grows after reionisation quenching takes place. Like previous simulations-based results, we find the size of the scatter increases with decreasing halo mass, beginning at the mass scale where reionisation quenches low-mass dwarfs. This is due to the increasing dominance of dark haloes (i.e. those devoid of stars) accreted by haloes of decreasing mass. The scatter at the high mass end, where reionisation does not quench galaxies, does not evolve significantly.
- While we do not find a significant break in the slope of the SMHM, one can be introduced if we push reionisation quenching to earlier times than in our default model. The break occurs at the boundary where reionisation begins to quench low-mass dwarfs. If a knee exists, the location of the knee, as well as the slopes above and below it, could help constrain the timing of reionisation and the mass scale at which dwarf galaxies are quenched.
- The two orders of magnitude difference between the location, slope, and scatter in the SMHM relation predicted by different hydrodynamical simulations occurs at the mass scale of reionisation relics. Reducing uncertainties on the subgrid physics that govern the formation of dwarf galaxies before reionisation, and uncertainties in the reionisation model, is likely key to understanding the true form of the SMHM.

Models that have explored the SMHM relation at lower masses have found intriguing signs of a flattening, likely a signature of H_2 cooling (e.g. Manwadkar & Kravtsov 2022; Ahvazi et al. 2024). While we currently do not have the resolution to model galaxies down to this regime, our $\langle \text{SFR} \rangle - v_{\max}$ relation appears to exhibit a flattening for small haloes, which may reproduce the trend in stellar masses. We are currently in the process of running a higher resolution suite of haloes at lower mass scales, which will enable us to study the SMHM relation in the ultra-low mass regime.

Assembly histories—and thus the SMHM relation—depend on the background cosmology. Alternative dark matter models such as warm dark matter predict different assembly history statistics (e.g. Ludlow et al. 2016), which should then map onto systematic differences in the SMHM. We are currently testing whether DarkLight needs recalibration to be applied to Λ WDM cosmologies.

Stellar mass is not the only property affected by the assembly history of a galaxy. Later assembly may produce lower stellar masses in addition to larger galaxy sizes and lower metallicities (Rey et al. 2019). As such, the scatter in each of these properties may not be fully independent, and galaxy formation models that assign galaxy properties treating each the scatter in each of these properties as independent may miss correlations that could be harnessed to improve dark matter constraints from up-coming surveys. We are currently implementing the dependence on assembly histories for galaxy sizes (Nigudar et al., in prep) and HI content (Hutton et al., in prep) into DarkLight, and plan to expand it to include also metallicities, kinematics, and shapes.

ACKNOWLEDGEMENTS

SYK thanks Annika Peter, Niusha Ahvazi, Andrew Benson, Ethan Nadler, Yao-Yuan Mao, and Marla Geha for helpful discussions that improved this manuscript. JIR would like to acknowledge support from STFC grants ST/Y002865/1 and ST/Y002857/1. MR is supported by the Beecroft Fellowship funded by Adrian Beecroft. MO acknowledges funding from the European Research Council (ERC) under the European Union’s Horizon 2020 research and innovation programme (grant agreement No. 852839). ET acknowledges the UKRI Science and Technology Facilities Council (STFC) for support (grant ST/V50712X/1). OA acknowledges support from the Knut and Alice Wallenberg Foundation, the Swedish Research Council (grant 2019-04659), and the Swedish National Space Agency (SNSA Dnr 2023-00164). This work was performed using the DiRAC Data Intensive service at Leicester, operated by the University of Leicester IT Services, which forms part of the STFC DiRAC HPC Facility (www.dirac.ac.uk). The authors acknowledge the use of the University of Surrey Eureka supercomputer.

Software: `pynbody` (Pontzen et al. 2013), `tangos` (Pontzen & Tremmel 2018), `colossus` (Diemer 2018), `SciPy` (Jones et al. 2001), `Matplotlib` (Hunter 2007), `NumPy` (van der Walt et al. 2011), `Jupyter` (jupyter.org).

AUTHOR CONTRIBUTIONS

Contributions from the authors were, based on the CRediT (Contribution Roles Taxonomy) system: **SK**: conceptualization; investigation; methodology; software; formal analysis; visualisation; writing - original draft, review & editing. **JR**: conceptualization; methodology; validation and interpretation; writing - original draft, review & editing; funding acquisition; project administration. **MR**: data curation; software; resources; writing - review & editing. **MO**: data curation; software; formal analysis; writing - review & editing. **SN**: investigation; methodology; formal analysis; software. **AP**: data curation; software; writing - review & editing. **ET**: data curation. **OA**: data curation; software; writing - review & editing. **PD**: writing - review & editing.

APPENDIX A: CORRELATIONS WITH SFR

In Read et al. (2017), a tight correlation was found between the average star formation rate and the halo mass $\langle \text{SFR} \rangle - M_{200}$ for Local Group dwarf galaxies. We test whether this holds for simulated galaxies in EDGE and a larger sample of observed, nearby isolated galaxies (see Sec. 2.1 for details on these datasets). In Fig. A1, we show the correlation between the mean star formation rate, $\langle \text{SFR} \rangle$ and halo mass, M_{200} . As in Fig. 1, we show pre-reionisation values in black and post-reionisation values in blue, and data from simulations with stars and from data in circles. While a correlation between $\langle \text{SFR} \rangle$ and M_{200} does exist, it has significantly larger scatter and uncertainties than it does with the peak rotation speed, v_{max} (see Figure A1). For this reason, we use instead the $\langle \text{SFR} \rangle - v_{\text{max}}$ relation in DarkLight.

APPENDIX B: V_{MAX} IN DMO VS BARYONIC SIMULATIONS

Here, we show that a suppression in v_{max} from dark matter only simulations better reproduces the v_{max} from its corresponding hydro-

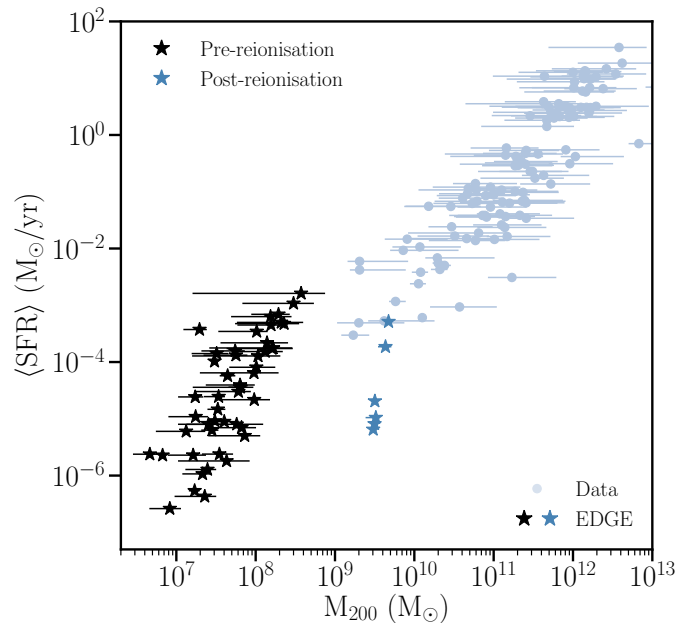


Figure A1. Relation between the average star formation rate and halo mass, M_{200} . There is significantly more scatter and larger uncertainties in the data than with v_{max} (c.f. Fig. 1). We thus use the $\langle \text{SFR} \rangle - v_{\text{max}}$ relation in DarkLight.

drodynamic simulation. In Fig. B1, we plot in red the v_{max} from hydrodynamic simulations (y-axis) against that from the DMO simulation (x-axis) for the same haloes. The solid black line denotes a 1-to-1 match between the v_{max} in both simulations, while the dashed black line denotes a reduction in the DMO v_{max} by a factor of $\sqrt{1 - f_b}$, where f_b is the baryon fraction of the universe. We find that this reduction better matches the v_{max} from the hydrodynamic simulations. The suppression in v_{max} for low-mass haloes is due to loss of baryons due to reionization and stellar feedback (e.g. Sawala et al. 2016). Thus in DarkLight, we apply this correction in v_{max} when run on DMO simulations.

REFERENCES

- Agertz O., et al., 2020, *MNRAS*, 491, 1656
 Ahvazi N., Benson A., Sales L. V., Nadler E. O., Weerasooriya S., Du X., Bovill M. S., 2024, *MNRAS*, 529, 3387
 Albers S. M., et al., 2019, *MNRAS*, p. 2515
 Applebaum E., Brooks A. M., Christensen C. R., Munshi F., Quinn T. R., Shen S., Tremmel M., 2021, *ApJ*, 906, 96
 Aubert D., et al., 2018, *ApJ*, 856, L22
 Behroozi P. S., Wechsler R. H., Conroy C., 2013, *ApJ*, 770, 57
 Behroozi P., Wechsler R. H., Hearin A. P., Conroy C., 2019, *MNRAS*, 488, 3143
 Benitez-Llambay A., Frenk C., 2020, *MNRAS*, 498, 4887
 Benitez-Llambay A., Fumagalli M., 2021, *ApJ*, 921, L9
 Benson A. J., 2012, *New Astron.*, 17, 175
 Bose S., Deason A. J., Frenk C. S., 2018, *ApJ*, 863, 123
 Boylan-Kolchin M., Bullock J. S., Kaplinghat M., 2012, *MNRAS*, 422, 1203
 Chan T. K., Kereš D., Oñorbe J., Hopkins P. F., Muratov A. L., Faucher-Giguère C. A., Quataert E., 2015, *MNRAS*, 454, 2981
 Christensen C. R., Brooks A. M., Munshi F., Riggs C., Van Nest J., Akins H., Quinn T. R., Chamberland L., 2024, *ApJ*, 961, 236

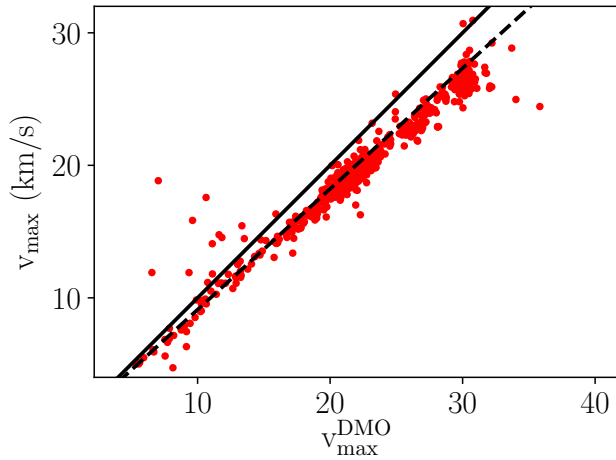


Figure B1. v_{\max} in the dark matter only (DMO) simulations plotted against that in the baryonic simulations. A perfect 1-to-1 match would lie along the black line; the dashed line represents multiplying the v_{\max} from the dark matter only sims by $\sqrt{1 - f_b}$, where $f_b = \Omega_b/\Omega_m = 0.17$ is the baryon fraction of the universe. This is a better match to the v_{\max} in the hydrodynamic simulations.

Cole S., Aragon-Salamanca A., Frenk C. S., Navarro J. F., Zepf S. E., 1994, *MNRAS*, **271**, 781

Cole A. A., Weisz D. R., Dolphin A. E., Skillman E. D., McConnachie A. W., Brooks A. M., Leaman R., 2014, *ApJ*, **795**, 54

Collins M. L. M., Read J. I., 2022, *Nature Astronomy*, **6**, 647

Danieli S., van Dokkum P., Conroy C., 2018, *ApJ*, **856**, 69

Danieli S., Greene J. E., Carlsten S., Jiang F., Beaton R., Goulding A. D., 2023, *ApJ*, **956**, 6

De Leo M., Read J. I., Noel N. E. D., Erkal D., Massana P., Carrera R., 2023, *arXiv e-prints*, p. [arXiv:2303.08838](https://arxiv.org/abs/2303.08838)

Diemer B., 2018, *ApJS*, **239**, 35

Eisenstein D. J., Hut P., 1998, *ApJ*, **498**, 137

Fitts A., et al., 2017, *Mon. Not. R. Astron. Soc.*, **471**, 3547

Garrison-Kimmel S., Boylan-Kolchin M., Bullock J. S., Lee K., 2014, *Mon. Not. R. Astron. Soc.*, **438**, 2578

Garrison-Kimmel S., Bullock J. S., Boylan-Kolchin M., Bardwell E., 2017, *MNRAS*, **464**, 3108

Genel S., et al., 2014, *MNRAS*, **445**, 175

Gibbons S. L. J., Belokurov V., Evans N. W., 2017, *MNRAS*, **464**, 794

Gray E. I., et al., 2024, *arXiv e-prints*, p. [arXiv:2405.19286](https://arxiv.org/abs/2405.19286)

Gutcke T. A., Pfrommer C., Bryan G. L., Pakmor R., Springel V., Naab T., 2022, *ApJ*, **941**, 120

Haardt F., Madau P., 1996, *ApJ*, **461**, 20

Hopkins P. F., et al., 2020, *MNRAS*, **492**, 3465

Hu C.-Y., et al., 2023, *ApJ*, **950**, 132

Hunter J. D., 2007, *Computing in Science and Engineering*, **9**, 90

Ibata R., Irwin M., Lewis G. F., Stolte A., 2001, *ApJ*, **547**, L133

Jeon M., Besla G., Bromm V., 2017, *ApJ*, **848**, 85

Jethwa P., Erkal D., Belokurov V., 2018, *MNRAS*, **473**, 2060

Jiang F., Dekel A., Freundlich J., van den Bosch F. C., Green S. B., Hopkins P. F., Benson A., Du X., 2021, *MNRAS*, **502**, 621

Jones E., Oliphant T., Peterson P., 2001

Katz H., et al., 2020, *MNRAS*, **494**, 2200

Keating L. C., Weinberger L. H., Kulkarni G., Haehnelt M. G., Chardin J., Aubert D., 2020, *MNRAS*, **491**, 1736

Kim S. Y., Peter A. H. G., Hargis J. R., 2018, *Phys. Rev. Lett.*, **121**, 211302

Klypin A., Kravtsov A. V., Valenzuela O., Prada F., 1999, *ApJ*, **522**, 82

Kravtsov A., Manwadkar V., 2022, *MNRAS*, **514**, 2667

Lelli F., McGaugh S. S., Schombert J. M., 2016, *AJ*, **152**, 157

Li T. S., et al., 2017, *ApJ*, **838**, 8

Li J., Greene J. E., Carlsten S. G., Danieli S., 2024, *arXiv e-prints*, p.

[arXiv:2406.00101](https://arxiv.org/abs/2406.00101)

Ludlow A. D., Bose S., Angulo R. E., Wang L., Hellwing W. A., Navarro J. F., Cole S., Frenk C. S., 2016, *MNRAS*, **460**, 1214

Manwadkar V., Kravtsov A. V., 2022, *MNRAS*, **516**, 3944

Mao Y.-Y., et al., 2024, *arXiv e-prints*, p. [arXiv:2404.14498](https://arxiv.org/abs/2404.14498)

Martin-Alvarez S., Sijacki D., Haehnelt M. G., Farcy M., Dubois Y., Belokurov V., Rosdahl J., Lopez-Rodriguez E., 2023, *Mon. Not. R. Astron. Soc.*, **525**, 3806

Moore B., Ghigna S., Governato F., Lake G., Quinn T., Stadel J., Tozzi P., 1999, *ApJ*, **524**, L19

Moster B. P., Naab T., White S. D. M., 2013, *MNRAS*, **428**, 3121

Moster B. P., Naab T., White S. D. M., 2018, *MNRAS*, **477**, 1822

Muni C., Pontzen A., Read J. I., Agertz O., Rey M. P., Taylor E., 2024, *arXiv e-prints*, p. [arXiv:2407.14579](https://arxiv.org/abs/2407.14579)

Munshi F., Brooks A. M., Applebaum E., Weisz D. R., Governato F., Quinn T. R., 2017, *arXiv e-prints*, p. [arXiv:1705.06286](https://arxiv.org/abs/1705.06286)

Munshi F., Brooks A. M., Christensen C., Applebaum E., Holley-Bockelmann K., Quinn T. R., Wadsley J., 2019, *ApJ*, **874**, 40

Munshi F., Brooks A. M., Applebaum E., Christensen C. R., Quinn T., Sligh S., 2021, *Astrophys. J.*, **923**, 35

Nadler E. O., et al., 2020, *ApJ*, **893**, 48

O'Leary J. A., Steinwandel U. P., Moster B. P., Martin N., Naab T., 2023, *MNRAS*, **520**, 897

Ocvirk P., et al., 2020, *MNRAS*, **496**, 4087

Oman K. A., Navarro J. F., Sales L. V., Fattahi A., Frenk C. S., Sawala T., Schaller M., White S. D. M., 2016, *MNRAS*, **460**, 3610

Orkney M. D. A., et al., 2021, *MNRAS*, **504**, 3509

Ou X., et al., 2024, *ApJ*, **966**, 33

Pace A. B., Erkal D., Li T. S., 2022, *ApJ*, **940**, 136

Peng Y.-j., et al., 2010, *ApJ*, **721**, 193

Planck Collaboration et al., 2014, *A&A*, **571**, A16

Pontzen A., Tremmel M., 2018, *ApJS*, **237**, 23

Pontzen A., Roškar R., Stinson G. S., Woods R., Reed D. M., Coles J., Quinn T. R., 2013, pynbody: Astrophysics Simulation Analysis for Python

Posti L., Fraternali F., Marasco A., 2019, *A&A*, **626**, A56

Read J. I., Erkal D., 2019, *MNRAS*, **487**, 5799

Read J. I., Iorio G., Agertz O., Fraternali F., 2017, *MNRAS*, **467**, 2019

Read J. I., Walker M. G., Steger P., 2019, *MNRAS*, **484**, 1401

Rey M. P., Starkenburg T. K., 2022, *MNRAS*, **510**, 4208

Rey M. P., Pontzen A., Agertz O., Orkney M. D. A., Read J. I., Saintonge A., Pedersen C., 2019, *ApJ*, **886**, L3

Rey M. P., Pontzen A., Agertz O., Orkney M. D. A., Read J. I., Rosdahl J., 2020, *MNRAS*, **497**, 1508

Rey M. P., Pontzen A., Agertz O., Orkney M. D. A., Read J. I., Saintonge A., Kim S. Y., Das P., 2022, *MNRAS*, **511**, 5672

Richstein H., et al., 2024, *arXiv e-prints*, p. [arXiv:2402.08731](https://arxiv.org/abs/2402.08731)

Rodríguez-Puebla A., Primack J. R., Avila-Reese V., Faber S. M., 2017, *MNRAS*, **470**, 651

Roth N., Pontzen A., Peiris H. V., 2016, *MNRAS*, **455**, 974

Sawala T., et al., 2016, *Mon. Not. R. Astron. Soc.*, **457**, 1931

Schaye J., et al., 2015, *MNRAS*, **446**, 521

Simon J. D., 2019, *ARA&A*, **57**, 375

Simon J. D., et al., 2021, *ApJ*, **908**, 18

Skillman E. D., et al., 2014, *ApJ*, **786**, 44

Teyssier R., 2002, *Astron. Astrophys. Suppl. Ser.*, **385**, 337

Tomozeiu M., Mayer L., Quinn T., 2016, *ApJ*, **827**, L15

Ural U., Wilkinson M. I., Read J. I., Walker M. G., 2015, *Nature Communications*, **6**, 7599

Vale A., Ostriker J. P., 2004, *MNRAS*, **353**, 189

Wang L., Dutton A. A., Stinson G. S., Macciò A. V., Penzo C., Kang X., Keller B. W., Wadsley J., 2015, *MNRAS*, **454**, 83

Wang Y., Nadler E. O., Mao Y.-Y., Adhikari S., Wechsler R. H., Behroozi P., 2021, *ApJ*, **915**, 116

Wang Y. R., et al., 2024, in American Astronomical Society Meeting Abstracts, p. 448.05D

Weisz D. R., Boylan-Kolchin M., 2017, *MNRAS*, **469**, L83

Weisz D. R., et al., 2012, *ApJ*, **748**, 88

- Wetzel A. R., Hopkins P. F., Kim J.-H., Faucher-Giguère C.-A., Kereš D., Quataert E., 2016, [ApJL](#), 827, L23
- Wheeler C., Oñorbe J., Bullock J. S., Boylan-Kolchin M., Elbert O. D., Garrison-Kimmel S., Hopkins P. F., Kereš D., 2015, [Mon. Not. R. Astron. Soc.](#), 453, 1305
- Wright A. C., Brooks A. M., Weisz D. R., Christensen C. R., 2019, [MNRAS](#), 482, 1176
- Zhang H.-X., Hunter D. A., Elmegreen B. G., Gao Y., Schruba A., 2012, [AJ](#), 143, 47
- Zoutendijk S. L., et al., 2021, [arXiv e-prints](#), p. [arXiv:2112.09374](#)
- van der Walt S., Colbert S. C., Varoquaux G., 2011, [Computing in Science and Engineering](#), 13, 22